In utero alcohol exposure impairs vessel-associated positioning and differentiation of oligodendrocytes in the developing neocortex

M. Brosolo, M. Lecointre, A. Laquerrière, F. Janin, D. Genty, A. Lebon, C. Lesueur, D. Vivien, S. Marret, F. Marguet, et al.

Neurobiology of Disease 171 (2022) 105791

Contents lists available at ScienceDirect

Neurobiology of Disease

journal homepage: www.elsevier.com/locate/ynbdi

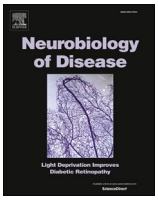

In utero alcohol exposure impairs vessel-associated positioning and differentiation of oligodendrocytes in the developing neocortex

M. Brosolo [a], M. Lecointre [a], A. Laquerrière [a,b], F. Janin [a], D. Genty [b], A. Lebon [c], C. Lesueur [a], D. Vivien [d,e], S. Marret [a,f], F. Marguet [a,b], B.J. Gonzalez [a,*]

[a] Normandie Univ, UNIROUEN, INSERM U1245, Normandy Centre for Genomic and Personalized Medicine, F 76000 Rouen, France
[b] Department of Pathology, Rouen University Hospital, 76000 Rouen, France
[c] Normandie Univ, UNIROUEN, INSERM US 51, CNRS UAR 2026, HeRacLeS-PRIMACEN, 76000 Rouen, France
[d] Normandie Univ, UNICAEN, INSERM UMR-S U1237, Physiopathology and Imaging of Neurological Disorders (PhIND), GIP Cyceron, Institut Blood and Brain @ Caen-Normandie (BB@C), 14000 Caen, France
[e] Department of Clinical Research, Caen-Normandie University Hospital, CHU, Avenue de la côte de Nacre, Caen, France
[f] Department of Neonatal Pediatrics and Intensive Care, Rouen University Hospital, 76000 Rouen, France

ARTICLE INFO

Keywords:
FASD
Vasculature
Cell migration
Cortical development
MBP

ABSTRACT

Prenatal alcohol exposure (PAE) is a major cause of nongenetic mental retardation and can lead to fetal alcohol syndrome (FAS), the most severe manifestation of fetal alcohol spectrum disorder (FASD). FASD infants present behavioral disabilities resulting from neurodevelopmental defects. Both grey and white matter lesions have been characterized and are associated with apoptotic death and/or ectopic migration profiles. In the last decade, it was shown that PAE impairs brain angiogenesis, and the radial organization of cortical microvessels is lost. Concurrently, several studies have reported that tangential migration of oligodendrocyte precursors (OPCs) originating from ganglionic eminences is vascular associated. Because numerous migrating oligodendrocytes enter the developing neocortex, the present study aimed to determine whether migrating OPCs interacted with radial cortical microvessels and whether alcohol-induced vascular impairments were associated with altered positioning and differentiation of cortical oligodendrocytes. Using a 3D morphometric analysis, the results revealed that in both human and mouse cortices, 15 to 40% of Olig2-positive cells were in close association with radial cortical microvessels, respectively. Despite perinatal vascular disorganization, PAE did not modify the vessel association of Olig2-positive cells but impaired their positioning between deep and superficial cortical layers. At the molecular level, PAE markedly but transiently reduced the expression of CNPase and MBP, two differentiation markers of immature and mature oligodendrocytes. In particular, PAE inverted their distribution profiles in cortical layers V and VI and reduced the thickness of the myelin sheath of efferent axons. These perinatal oligo-vascular defects were associated with motor disabilities that persisted in adults. Altogether, the present study provides the first evidence that Olig2-positive cells entering the neocortex are associated with radial microvessels. PAE disorganized the cortical microvasculature and delayed the positioning and differentiation of oligodendrocytes. Although most of these oligovascular defects occurred in perinatal life, the offspring developed long-term motor troubles. Altogether, these data suggest that alcohol-induced oligo-vascular impairments contribute to the neurodevelopmental issues described in FASD.

1. Introduction

Despite public health messaging, approximately 10% of women worldwide consume alcohol during their pregnancy (Popova et al., 2019). Prenatal alcohol exposure (PAE) represents a major cause of nongenetic mental retardation, making alcohol consumption during pregnancy an extremely important public health concern (Lange et al., 2017). Indeed, PAE can cause fetal alcohol syndrome (FAS), the most severe manifestation of fetal alcohol spectrum disorders (FASD; Riley et al., 2011). FAS is characterized by a large set of physical and mental

Abbreviations: FAS, Fetal alcohol syndrome; FASD, Fetal alcohol spectrum disorder; PAE, Prenatal alcohol exposure; OPC, Oligodendrocyte precursor.

* Corresponding author.
E-mail address: bruno.gonzalez@univ-rouen.fr (B.J. Gonzalez).

https://doi.org/10.1016/j.nbd.2022.105791
Received 15 April 2022; Received in revised form 30 May 2022; Accepted 10 June 2022
Available online 26 June 2022

disorders, including intrauterine growth retardation, craniofacial dysmorphism, neurodevelopmental defects and neurobehavioral troubles, such as learning or attention deficits (Riley et al., 2011). Although most FASD children frequently express life-long behavioral disabilities similar to FAS, they do not present morphological dysmorphism, leading to delayed diagnosis and medical care (Chasnoff et al., 2015).

At any stage of gestation, alcohol can be harmful, and even if it impacts numerous organs and cell types, its deleterious effects are highly noxious for the developing brain (Sulik, 2014). In particular, based on clinical research and animal model studies, PAE alters oligodendrocyte morphology and survival (Creeley et al., 2013; Dalitz et al., 2008; Newville et al., 2017). Thereby, Dalitz and coworkers identified attenuated processes and altered oligodendrocyte cell bodies in the brains of sheep fetuses exposed to alcohol *in utero* (Dalitz et al., 2008). Similarly, the Olney group showed that in macaque fetuses, PAE induces oligodendrocyte apoptosis (Creeley et al., 2013). Furthermore, it is well established that *in utero* alcohol exposure can lead to persistent white matter abnormalities, leading to corpus callosum deformities visualized using diffusion tensor imaging both in rodents and humans (Newville et al., 2017; Wozniak et al., 2009).

Beyond the main role of oligodendrocytes in improving neuronal signal conduction along myelinated axons in the mature brain (Barateiro et al., 2016), a tight cell–cell interaction has been recently evidenced in the developing brain between microvessels and oligodendrocytes (Yuen et al., 2014). Indeed, in addition to their functions of oxygen, trophic factors and nutrient supply, it is now established that cortical microvessels constitute physical support for nervous cell migration (Segara et al., 2019). First described for GABAergic interneurons (Won et al., 2013), Tsai and coworkers more recently showed that oligodendrocytes constitute a second population of migrating nervous cells using a vessel-associated process (Tsai et al., 2016). In particular, oligodendrocyte precursors migrate tangentially to reach the developing corpus callosum (Tsai et al., 2016). Consistent with these neurodevelopmental data, *in vitro* studies previously showed that growth factor production by endothelial cells, such as BDNF or VEGF, is involved in the proliferation and survival of oligodendrocytes (Aria et al., 2009). Jointly, oligodendrocytes promote vascular remodeling in white matter (Myamoto et al., 2014). Altogether, these data suggested that, as recently shown for GABAergic interneurons (Léger et al., 2020a), oligodendrocytes invading the cortical layers migrate along radial microvessels.

Several *in vivo* studies performed in adult mice and nonhuman primates showed that alcohol affects angiogenesis and vasculogenesis by altering wound healing and new vessel formation (Radek et al., 2005; Williams et al., 2008). *In vitro,* ethanol has also been shown to disrupt VEGF receptor signaling in cultured endothelial cells (Radek et al., 2008). More recently, *in vitro* and *in vivo* studies performed in the developing brain have demonstrated that alcohol impairs brain angiogenesis, causing a loss of the radial organization of cortical microvessels, dysfunction of endothelial MMP9 activity and disruption of the vessel-associated migration of GABAergic interneurons (Jégou et al., 2012; Léger et al., 2020a and 2020b). At a mechanistic level, these effects are associated with deregulation of the expression of VEGF receptor 1 (VEGFR1) and the endothelial NMDA receptor (Léger et al., 2020a). These deleterious effects of *in utero* alcohol exposure on the cortical vasculature and the mispositioning of GABA interneurons were also described in human fetuses (Jégou et al., 2012; Marguet et al., 2020). However, the effect of PAE on oligovascular interactions remains unexplored.

Given the critical role of oligodendrocytes in neuronal signal conduction (Jäkel and Dimou, 2017), the recently described vessel-associated migration of oligodendrocytes in the developing corpus callosum (Tsai et al., 2016) and our recent data showing that alcohol impairs cortical angiogenesis and endothelial activity (Léger et al., 2020a and 2020b), we hypothesized that PAE would impair the vessel-associated positioning of migrating oligodendrocytes invading the developing cortex and the maturation of the oligodendrocytic lineage. For this purpose, first, we researched oligovascular interactions in the developing cortex of human fetuses and, second, used a mouse model of FASD to *(i)* assess the effects of alcohol on oligovascular interactions and oligodendrocyte positioning on cortical layers, *(ii)* characterize the impact of prenatal alcohol exposure on oligodendrocyte maturation stages and *(iii)* determine whether such neurodevelopmental defects are associated with perinatal and adult behavioral troubles.

2. Materials and methods

2.1. Control and alcohol-exposed human brains

In agreement with the local ethics committee and French laws, the fetal brains used in this study (Fig. 1A) belong to a collection that has been declared to the French Ministry of Health (Collection number DC-2015-2468, cession number AC-2015-2467, located in A. Laquerrière's Pathology Laboratory, Rouen University Hospital). Every case was obtained with the written consent of the parents, and autopsy procedures were performed according to standardized protocols. The clinical characteristics and cause of death of the control and FAS patients are presented in Table 1.

2.2. In vivo treatment of pregnant and lactating mice

NMRI (Naval Medical Research Institute) mice were purchased from Janvier (Le Genest Saint Isle, France). Mice were kept in a temperature-controlled room (21 ± 1 °C) with a 12 h/12 h light/dark cycle (lights on from 7 a.m. to 7 p.m.) and free access to food and tap water. Pregnant NMRI mice received a daily subcutaneous injection of 0.9% NaCl or 3 g/kg ethanol diluted 50% vol/vol in 0.9% NaCl, from gestational Day 15 (GD15) to GD20 (Fig. 1B). At parturition day (P0) and one day after parturition (P1), mothers received a daily injection of the same composition (Jégou et al., 2012; Lecuyer et al., 2017; Léger et al., 2020b). The administered dose of ethanol was based on a previous study (Jégou et al., 2012) and resulted in a blood alcohol level (BAL) of 1.5 g/L 30 min after the injection. This BAL value, which is representative of drunkenness in humans, was <0.5 g/L after 3 h. Mice were used according to the French Ethical Committee recommendations and European directives 2010/63/UE, and experiments were performed under the supervision of authorized investigators (authorization no. APAFIS#22136–2,019,092,013,438,607 v4 from the Ministère de l'Agriculture et de la Pêche).

For immunohistochemistry, qRT–PCR and western blot experiments targeting differentiation markers of the oligodendrocyte lineage, brains from fetuses and pups were collected at embryonic Day 20 (E20), postnatal Day 2 (P2), P15 and P45. E20 and P2 stages were chosen to cover the progressive arrival in the neocortex of the different waves of oligodendrocyte precursors generated in ganglionic eminences and the dorsal periventricular zone (Van Tilborg et al., 2018). P15 was selected since, at this stage, the cortical positioning of oligodendrocytes is almost established although differentiation is not (Nishiyama et al., 2021). The P45 (young adult) stage was selected since positioning and maturation is completed.

In order to reduce the risk of litter effect, experiments were managed as follow: for histological and morphometric analysis, experiments were conducted in slices from different neonates from different litters. For qRT-PCR and western blot experiments, extracts were from different litters from independent treatments. For behavioral studies, mice were from different litters from independent treatments.

2.3. Quantitative reverse transcriptase polymerase chain reaction

From E20, P2 and P15 *in utero*-exposed cortices, RNA was column-purified according to the manufacturer's guidelines (Macherey-Nagel, Germany). After DNase digestion, cDNA was prepared from 1 μg total RNA using random primers and Avian Myeloblastosis Virus Reverse

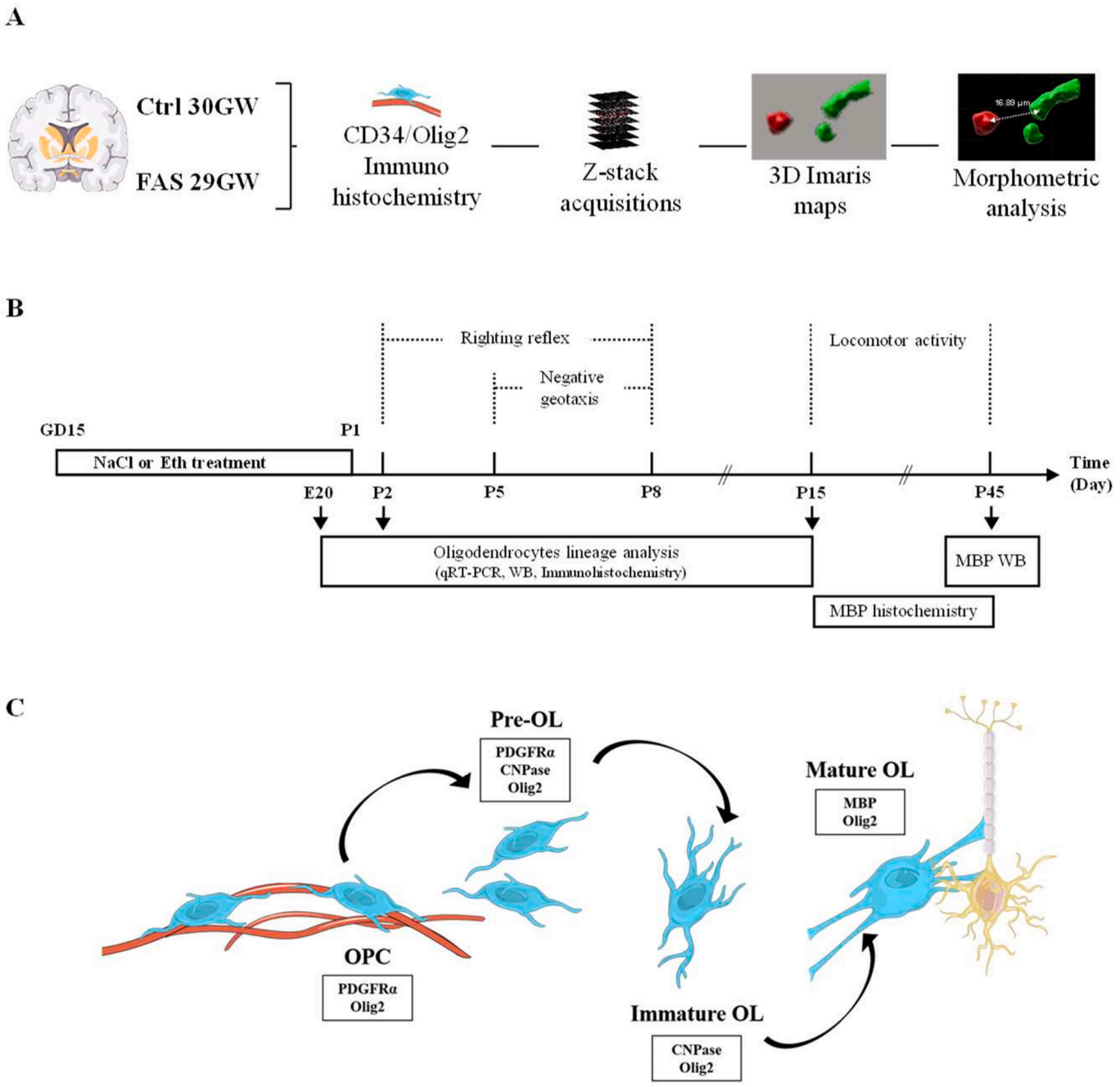

Fig. 1. A, B. Graphical description of the experiments conducted in human brains from control and alcohol-exposed fetuses (A) and in the preclinical model of FASD (B). C. Maturation markers used in the study that are representative of the four main stages of oligodendrocyte differentiation described in the literature (Marinelli et al., 2016). CD34: Cluster of differentiation 34; CNPase: 2′,3′-Cyclic-nucleotide 3′-phosphodiesterase; Eth: Ethanol; Ex: Embryonic Day x; GD15: gestational Day 15; GW: gestational weeks; MBP: myelin basic protein; Olig2: oligodendrocyte transcription factor 2; OL: oligodendrocyte; OPC: oligodendrocyte progenitors cells; PDGFRα: platelet-derived growth factor-α; Pre-OL: preoligodendrocytes; Px: postnatal Day x; qRT–PCR: reverse transcription polymerase chain reaction; WB: western blot.

Transcriptase (Promega, Madison). A master mix was prepared using sense and antisense primers (Invitrogen; Table 2) and SYBR Green PCR Mix (Bio–Rad). Using a LightCycler® 96 W1.1 machine (Roche; Bâle, Suisse), PCRs were performed using the following cycle conditions: 95 °C (180 s), 95 °C (10 s) and 60 °C (30 s) for 40 cycles, 95 °C (10 s), 65 °C (60 s) and 97 °C (1 s). The comparative threshold cycle (Ct) method was used, and the cDNA amount in the sample was expressed as $2^{-\Delta\Delta Ct}$ using glyceraldehyde-3-phosphate dehydrogenase (GAPDH) as an internal control. The GAPDH mRNA level was not affected by ethanol treatment.

2.4. Analysis by western blot of cortical extracts from mice

Cortical extracts from control and *in utero* alcohol-exposed animals were microdissected and homogenized in ice-cold lysis buffer. Fifty micrograms of protein extracts, as determined by the Bradford assay, were denatured at 100 °C for 5 min in Laemmli buffer (Tris-HCl 0.5 M; pH 6.8; SDS 8%; bromophenol blue 0.5%; glycerol 10%; β-mercaptoethanol 10%) and loaded onto a 10% SDS-polyacrylamide gel. After separation, proteins were electrically transferred onto a nitrocellulose membrane (Bio–Rad Laboratories, Marne la Coquette, France). The

Table 1
Clinical and morphological characteristics of control and alcohol exposed fetuses.

Cases	Term	Morphological characteristics	Cause of death
Control case	30 GW	None	Cord prolapse
FAS case	29 GW	Anteversed nostrils and pointed nose Ear anomalies Indistinct philtrum	*In utero* fetal death
		Retrognathism	Cardiopathy

Table 2
Primers used for qRT–PCR experiments. GAPDH was used as internal control.

Primers	Sequences 5′ to 3′
PDGFRα *f*	GACGTTCAAGACCAGCGAGTT
PDGFRα *r*	CAGTCTGGCGTGCGTCC
CNPase *f*	AGACAGCGTGGCGACTAGACT
CNPase *r*	GGGCTTCAGCTTCTTCAGGT
MBP *f*	ACGAGAACTACCCATTATG
MBP *r*	GATGGAGGTGGTGTTC
Olig2 *f*	AGCCAGGTTCTCCTC
Olig2 *r*	GGGCAGAAAAAGATCATC
GAPDH *f*	CCTGCTTCACCACCTTCTTGA
GAPDH *r*	CATGGCCTTCCGTGTTCCTA

membrane was incubated with blocking solution (5% BSA or 5% milk in Tris-buffered saline containing 0.05% Tween 20) at room temperature for 1 h and incubated overnight with primary antibodies (Table 3). After incubation with the corresponding secondary antibody coupled to peroxidase (Santa Cruz Biotechnology, Santa Cruz, CA), proteins were visualized using an enhanced chemiluminescence (ECL) immunoblotting detection system (Biorad Laboratories, Marne la Coquette, France). The intensity of the immunoreactive bands was quantified using a blot analysis system (Bio–Rad Laboratories, Marne la Coquette, France), and β-actin was used as a loading control. Commercial markers (Seeblue prestained standard; Invitrogen) were used as molecular weight standards.

2.5. Immunohistochemistry

In mice, brain sections previously fixed with 4% PFA in PBS were incubated overnight at 4 °C with various primary antibodies (Table 3) diluted in incubation buffer (PBS containing 1% BSA and 3% Triton X-100). Slices were rinsed thrice with PBS for 10 min and incubated with the same incubation buffer containing the appropriate secondary antibody. By omitting the primary antibodies, a control for nonspecific binding of the secondary antibody was performed. Immunolabeled slices were visualized using a Leica DMI 600B, Thunder Imaging System CTR5500 or Leica TCS SP8 MP confocal microscope. Analyses were performed using the *FIJI Is Just Image J* (FIJI) software.

In humans, immunohistochemistry was performed on 6-µm dewaxing brain sections according to standardized protocols in mice.

2.6. Quantification of the immunoreactive profiles of differentiation markers of oligodendrocytes in cortical layers

Measurements of immature and mature oligodendrocyte immunoreactive profiles in cortical layers were performed after immunostaining of P15 slices with CNPase and MBP antibodies, respectively (Table 3). After 10× magnification acquisitions, quantification of CNPase or MBP fluorescent intensity profiles in the developing cortex was performed in animals prenatally exposed to NaCl or ethanol using the “line scan” tool of the Metamorph® software (Roper Scientific, Downingtown, USA). Then, the area under the curve of each cortical layer was evaluated. For a given cortex, a comparison of the distribution pattern of CNPase (immature oligodendrocyte) and MBP (mature oligodendrocyte) was then performed.

2.7. Quantification of the Olig2-positive cell density in the developing cortical layers and corpus callosum

Measurement of the density of oligodendrocytes in cortical layers and corpus callosum was performed after immunostaining of E20, P2 and P15 slices using the Olig2 antibody (Table 3). Images were acquired at 10× magnification, and regions of interest (ROIs) were defined within the deep cortical layers (DCL), the superficial cortical layers (SCL) and the corpus callosum. Definition of DCL and SCL evolved with the developmental stage as follow: at E20, DCL consisted in the maturing layer VI and SCL in the cortical plate; at P2, DCL consisted in layer VI and maturing layer V and SCL in the cortical plate; at P15, DCL consisted in layer VI and V and SCL in the layers IV to I. Fluorometric analysis using the multipoint counting tool of the FIJI software gave access to the number of immunoreactive cells present in the ROI. Density was then determined by a ratio between the number of cells and the ROI area. The analysis was repeated to cover the corpus callosum and the superficial and deep cortical layers in both hemispheres and in three slices per animal (Léger et al., 2020a).

Table 3
Antibodies used for immunohistochemitry and western blot experiments.

Antibodies	Trade reference	Purified species	Supplier	Dilution	Solution of incubation
CD31/PECAM	IHC: cat 550,274	Rat	BD-Pharmigen	1/200	1% BSA, 3% Triton X-100 in PBS
CD34	IHC: 790–2927	Mouse	ROCHE	Prediluted	1% BSA, 3% Triton X-100 in PBS
CNPase	IHC: NB100–1935	Chicken	Novus Biological	1/200	IHC: 1% BSA, 3% Triton X-100 in PBS WB: BSA (5% TBST)
	WB: Ab227218	Rabbit	Abcam	1/1000	
GFAP	IHC: Ab10062	Mouse	Abcam	1/200	1% BSA, 3% Triton X-100 in PBS
Glut1	IHC: SC 1605	Goat	Santa Cruz	1/200	1% BSA, 3% Triton X-100 in PBS
MBP	IHC: Ab7349	Rat	Abcam	1/200	IHC: 1% BSA, 3% Triton X-100 in PBS WB: BSA (5% TBST)
	WB: Ab7349			1/1000	
Olig2	IHC: Ab136253	Rabbit	Abcam	1/200	IHC: 1% BSA, 3% Triton X-100 in PBS WB: BSA (5% TBST)
	WB: Ab136253			1/1000	
PDGFRα	IHC: AF1062	Goat	R&D System	1/200	IHC: 1% BSA, 3% Triton X-100 in PBS WB: BSA (5% TBST)
	WB: PA5–16571	Rabbit	ThermoFisher	1/1000	
β-Actin	WB: A5441	Mouse	Sigma- Aldrich	1/5000	Milk (5% in TBST)

2.8. Measurement of microvascular organization and oligo-vascular interactions in the developing cortex

The quantification of the angular orientation of cortical microvessels was performed in the frontoparietal cortex of control and alcohol-exposed mice at E20, P2 and P15 as previously described (Jégou et al., 2012). Practically, a frame of lines was defined perpendicular to the cortical border (radial orientation). For microvessels parallel to these lines, the Metamorph Software arbitrarily attributed the angular value 0°. The maximal angular value affected was 90°. Angle values of cortical microvessels were then distributed in four classes [0–25°[, [25–50°[, [50–75°[and [75–90°[.

The quantification of vessel-associated oligodendrocytes was performed in human and mouse brain slices after double immunostaining with Olig2 (oligodendrocytic lineage) and CD31, Glut1 or CD34 (endothelial cells) antibodies (Table 3). In humans, experiments were conducted on a control fetal brain at GW30 and on a FAS fetal brain at GW29. In mice, experiments were performed in cortex slices at E20, P2 and P15. Z stack acquisitions were performed and saved in TIFF format using a Leica TCS SP8 MP confocal microscope. Afterward, the *Z*-stack series of images was loaded into IMARIS imaging software 9.0.2 (Bitplane, Zurich, Switzerland) for 3D reconstruction (Videos S1 and S2). To validate a vessel-oligodendrocyte interaction, the maximal distance between the center part of Olig2-positive cells and the center part of the vessel was fixed at 10 μm.

2.9. Quantification of MBP-positive fibers in the cortical layers and MBP-positive bundles in the striatum

After immunostaining of P15 mouse brain slices with MBP antibody (Table 3), high-resolution images were acquired at 10× magnification using a Thunder Imaging System CTR5500. Images were loaded in FIJI software, and thresholding of the immunoreactive MBP fibers was performed in each ROI of the cortex, giving access to the thresholded fiber area/ROI area ratio. Similarly, quantification of MBP-positive bundles was performed in the striatum at the same stage. Morphometric analysis provides access to the number of immunoreactive bundles per ROI area.

2.10. Electronic microscopy and quantification of axonal myelinated fibers and myelin sheath thicknesses in the corpus callosum at P15

Electron microscopy ultrastructural studies were performed according to standardized protocols (Roux et al., 2014). Briefly, cortices obtained from the P15 corpus callosum of neonates previously *in utero* exposed to NaCl or ethanol were fixed in a 2% glutaraldehyde solution, postfixed with 1% osmium tetroxide, and embedded in epoxy resin. Semithin sections were stained with toluidine blue, uranyl acetate and lead citrate to enhance contrast and examined under a PHILIPS CM10 electron microscope. Axonal myelinated fiber density and myelin sheath thickness in the corpus callosum were measured at P15 after electronic microscopy acquisitions at 120× and 295× magnification. FIJI software was used to determine to the area and number of objects (myelinated fibers) within the ROI and the ROI area ratio. This analysis was performed in four plans per animal. Myelin sheath thickness was evaluated using FIJI lines tools.

2.11. Behavioral evaluations

Each mouse was submitted to the same series of behavioral tests, respecting the same schedule to limit the potential confounding factors linked to animal manipulations. Following the last day of treatment, weight tracking was recorded daily from P2 to P10 and, subsequently, at P15 and P45 (Fig. S1). Because in humans, white matter lesions, such as leucomalacia, are frequently associated with motor disabilities (Volpe, 2009), behavioral tests were focused on sensorimotor impairments.

2.11.1. Behavioral evaluation of pup sensorimotor disabilities

From P2 to P8, the righting reflex test consists of the evaluation of a reflexive sensorimotor ability task (Daher et al., 2017; Syed et al., 2016). Practically, pups were placed supine on a plane surface, and their mean time to restore a normal prone position on two consecutive trials was noted. The cutoff time per trial was set at 60 s, and the value was the mean of 2 successive trials.

From P5 to P8, the negative geotaxis test is a vestibular and body coordination task (Daher et al., 2017; Syed et al., 2016). The animals were placed on a 20° tilted plane with their head facing downward, and the mean time to realize a full rotation of 180° and face up was measured in each group. The latency for a semi-rotation (90°) was also counted. The cutoff time per trial was set at 60 s.

2.11.2. Evaluation of locomotor activity

Locomotor activity of control and *in utero* alcohol-exposed mice was assessed at P15 and P45. At P45, the locomotor activity was measured using mice at the diestrus stage. Estrus cycle was monitored by visual observation of the vagina (Byers et al., 2012). Animals were isolated for 5 min in individual cages before being placed in individual 50 × 50 × 38 cm compartments in a sound-attenuated and temperature-regulated (20 ± 1 °C) room to limit anxiety. This test takes advantage of a rodent's natural tendency to explore a new environment. The recording apparatus was connected to a computer to process the data. Distance travelled was measured by video tracking using an EthoVision XT Logiciel (Noldus®) during a 30-min period. Data were expressed by 10-min segments and the whole recording period.

2.12. Statistical analysis

Statistical analyses were performed using the biostatistics Prism software (GraphPad® Software, La Jolla, CA). The tests used and *p values* are summarized in Tables 4 and 5. Error bars in the graphs represent SEM. Females and males were identified. However, when the results showed no sex differences, the data were pooled in the same figure. Unpooled data are provided in Supplementary Figs. 3, 4, 7, 8 and 9.

3. Results

3.1. Vessel association of Olig2-positive cells persists in human FAS cortices

Previous studies reported that PAE impairs the cortical vasculature in the developing human brain (Jégou et al., 2012). This effect, which is also observed in mice, is associated with dysfunction of cortical endothelial cells (Léger et al., 2020b). Because migrating oligodendrocytes use microvessels as guides (Tsai et al., 2016), we explored whether PAE altered the oligovascular association (Fig. 2). Double immunostaining experiments with Olig2 and CD34 antibodies were performed in a FAS 29GW fetus (Fig. 2A). Confocal acquisitions performed in the deep cortical layers demonstrated that some Olig2-positive cells were vessel-associated (Fig. 2B; arrows), whereas several other Olig2-positive cells were located at a distance (Fig. 2A, B; arrowhead). To validate the vessel association, *Z*-stack acquisitions were realized, and a 3D map was built (Fig. 2C-E). Rotation around the vessel axis and quantification of the oligo-vascular distances indicated that, in deep cortical layers, approximately 6% of the Olig2-positive cells were vessel associated (Fig. 2C-E; Fig. 2J; Video S1). Similarly, experiments were conducted in a control 30GW (Fig. 2F-H). Morphometric analysis showed that, as observed in the FAS case, several Olig2-positive cells were vessel associated (Fig. 2G, H; arrow). Quantitative analysis revealed a higher percentage of vessel-associated Olig2 cells in the control fetus (15.79%; Fig. 2I). Nevertheless, considering *i)* the scarcity of human tissues and *ii)* the frequent multi-intoxication profiles of human FAS fetuses, preclinical experiments were conducted using a mono-intoxication model of PAE.

Table 4
Main figures statistical analysis. The tests used, the number of independent experiments, the number of measures per experiment and p values are detailed for each experiments. Error bars in the graphs represent SEM.

Experiments	Test	n Independents experiments	p value *p < 0.05; **p < 0.01; ***p < 0.001; ****p < 0.0001
Fig. 3E Distribution of cortical vessels orientation at E20	Chi-square test	*n* = 5 at least 3 slices analysed from 5 independent animals per treatment	Chi-square, df 9.709, 3 p = 0.0212*
Fig. 3F Olig2-positive cells vessel associated at E20	Two way ANOVA Tukey post-test	n = 5 at least 3 slices analysed from 5 independent animals per treatment	ANOVA Interaction F 0.5432; *p* = 0.7594; ns Zones F 9.934; *p* = 0.2014; ns Treatment F 0.0022; *p* = 0.9844; ns
Fig. 3I Distribution of cortical vessels orientation at P2	Chi-square test	n = 5 at least 3 slices analysed from 5 independent animals per treatment	Chi-square, df 8.536, 3 p = 0.0361*
Fig. 3J Olig2-positive cells vessel associated at P2	Two way ANOVA Tukey post-test	n = 5 at least 3 slices analysed from 5 independent animals per treatment	ANOVA Interaction F 0.1072; *p* = 0.8721; ns Zones F 2.679; *p* = 0.4240; ns Treatment F 0.01191; *p* = 0.9572; ns
Fig. 3M Distribution of cortical vessels orientation at P15	Chi-square test	n = 5 at least 3 slices analysed from 5 independent animals per treatment	Chi-square, df 0.8597, 3 p = 0.8351; ns
Fig. 3N Olig2-positive cells vessel associated at P15	Two way ANOVA Tukey post-test	n = 5 at least 3 slices analysed from 5 independent animals per treatment	ANOVA Interaction F 0.0406; *p* = 0.9366; ns Zones F 0.09556; *p* = 0.9030; ns Treatment F 0.1317; *p* = 0.8862; ns
Fig. 4C Olig2-positive cells density in deep cortical layers (DCL)	Two way ANOVA Tukey post-test	n = 5 at least 3 slices analysed from 5 independent animals per treatment	ANOVA Interaction F 0.1787; ns Ages F 83.29; *p* < 0.0001**** Treatment F 0.1792; *p* = 0.5833; ns Tukey's E20 NaCl *vs* P2 NaCl *p* < 0.0001**** P2 NaCl *vs* P15 NaCl *p* < 0.0001****
Fig. 4D Olig2-positive cells density in superficial cortical layers (SCL)	Two way ANOVA Tukey post-test	n = 5 at least 3 slices analysed from 5 independent animals per treatment	ANOVA Interaction F 0.2338; ns Ages F 85.87; *p* < 0.0001**** Treatment F 0.5127; *p* = 0.3070; ns Tukey's E20 NaCl *vs* P2 NaCl *p* < 0.0001**** P2 NaCl *vs* P15 NaCl p < 0.0001**** ANOVA
Fig. 4E Ratio Olig2-positive SCL *vs* DCL in NaCl	One way ANOVA Tukey post-test	n = 5 at least 3 slices analysed from 5 independent animals per treatment	F 26.88; p < 0.0001**** Tukey's E20 NaCl *vs* P2 NaCl p < 0.0001**** E20 NaCl *vs* P15 NaCl p < 0.0001****
Fig. 4F Ratio Olig2-positive SCL *vs* DCL in Ethanol	One way ANOVA Tukey post-test	n = 5 at least 3 slices analysed from 5 independent animals per treatment	ANOVA F 32.53; p < 0.0001**** Tukey's E20 NaCl *vs* P2 NaCl p < 0.0001**** E20 NaCl *vs* P15 NaCl p < 0.0001****
Fig. 4G Ratio Olig2-positive SCL *vs* DCL at P2	Unpaired t-test	n = 5 at least 3 slices analysed from 5 independent animals per treatment	NaCl *vs* Eth *p* < 0.05*
Fig. 5A PDGFRα qRT–PCR on cortical extracts	Two way ANOVA Tukey post-test	n = 16 animals per age and per treatment Males = 8 Females = 8	ANOVA Interaction F 0.7139; *p* < 0.05* Ages F 88.81; *p* < 0.0001**** Treatment F 0.07787; *p* = 0.3898; ns Tukey's E20 NaCl *vs* P2 NaCl p < 0.0001**** E20 NaCl *vs* P15 NaCl p < 0.0001**** P2 NaCl *vs* P15 NaCl p < 0.0001****
Fig. 5B CNPase qRT–PCR on cortical extracts	Two way ANOVA Tukey post-test	n = 16 animals per age and per treatment Males = 8 Females = 8	ANOVA Interaction F 0.5603; ns Ages F 81.99; *p* < 0.0001**** Treatment F 0.2806; *p* = 0.2440; ns Tukey's E20 NaCl *vs* P15 NaCl *p* < 0.0001**** P2 NaCl *vs* P15 NaCl p < 0.0001****
Fig. 5C MBP	Two way ANOVA	n = 16 animals per age and per treatment	ANOVA Interaction F 2.643; *p* < 0.05*

(*continued on next page*)

Table 4 (*continued*)

Experiments	Test	n	p value
		Independents experiments	*p < 0.05; **p < 0.01; ***p < 0.001; ****p < 0.0001
qRT–PCR on cortical extracts	Tukey post-test	Males = 8 Females = 8	Ages F 69.65; $p < 0.0001$**** Treatment F 1.300; $P < 0.05$* Tukey's E20 NaCl *vs* P15 NaCl $p < 0.0001$**** P2 NaCl *vs* P15 NaCl $p < 0.0001$**** P15 NaCl *vs* P15 Eth $p < 0.01$** ANOVA Interaction F 0.4516; ns Ages F 87.84; $p < 0.0001$**** Treatment F 0.5053; $p = 0.0529$; ns Tukey's E20 NaCl *vs* P2 NaCl $p < 0.0001$**** P2 NaCl *vs* P15 NaCl p < 0.0001****
Fig. 5D Olig2 qRT–PCR on cortical extracts	Two way ANOVA Tukey post-test	n = 16 animals per age and per treatment Males = 8 Females = 8	
Fig. 5F Western blot PDGFRα on cortical extracts	Unpaired t-test	n = 16 animals per age and per treatment Males = 8 Females = 8	E20 NaCl *vs* E20 Eth $p = 0.1169$; ns P2 NaCl *vs* P2 Eth $p = 0.9255$; ns P15 NaCl *vs* P15 Eth $p = 0.5642$; ns
Fig. 5G Western blot CNPase on cortical extracts	Unpaired t-test	n = 16 animals per age and per treatment Males = 8 Females = 8	E20 NaCl *vs* E20 Eth $p < 0.05$* P2 NaCl *vs* P2 Eth p < 0.01** P15 NaCl *vs* P15 Eth $p = 0.1092$; ns
Fig. 5H Western blot MBP on P15 cortical extracts	Unpaired t-test	n = 16 animals per treatment Males = 8 Females = 8	P15 NaCl *vs* P15 Eth $p < 0.01$**
Fig. 5I Western blot Olig2 on cortical extracts	Unpaired t-test	n = 16 animals per age and per treatment Males = 8 Females = 8	E20 NaCl *vs* E20 Eth $p = 0.1349$; ns P2 NaCl *vs* P2 Eth $p = 0.4744$; ns P15 NaCl *vs* P15 Eth $p = 0.7280$; ns
Fig. 6D CNPase fluorescent intensity on cortical layers at P15	Unpaired t-test	n = 5 at least 5 measures per animals per treatment	P15 NaCl *vs* P15 Eth in cortical layers V; $p < 0.05$* P15 NaCl *vs* P15 Eth in cortical layers VI; p < 0.05*
Fig. 6H MBP fluorescent intensity on cortical layers at P15	Unpaired t-test	n = 5 at least 5 measures per animals per treatment	P15 NaCl *vs* P15 Eth in cortical layers VI; p < 0.05*
Fig. 6K MBP/CNPase ratio of fluorescent intensity on cortical layers at P15	Unpaired t-test	n = 5 at least 5 measures per animals per treatment	P15 NaCl *vs* P15 Eth in cortical layers VI; $p < 0.01$**
Fig. 7E Myelinated fibers density	Unpaired t-test	$n = 6$ at least 4 ROI analysed from 6 independent animals per treatment	NaCl *vs* Eth p < 0.05*
Fig. 7F Myelin sheath thickness	Unpaired t-test	n = 6 at least 4 ROI analysed from 6 independent animals per treatment	NaCl *vs* Eth $p < 0.001$***
Fig. 7G Distribution of axonal area	Chi-square test	n = 6 at least 4 ROI analysed from 6 independent animals per treatment	Chi-square, df 5.134, 4 $p = 0.2738$; ns
Fig. 8A Latency to turn in the righting reflex test over time	Two way ANOVA Tukey post-test	n = 37 in NaCl; $n = 37$ in Eth Females NaCl = 17 Females Eth = 18 Males NaCl = 20 Males Eth = 19	ANOVA F 8.347; $p < 0.0001$**** Ages F 29.45; p < 0.0001**** Treatment F 0.007081; $p = 0.8196$; ns Tukey's P2 NaCl *vs* P2 Eth p < 0.0001**** P6 NaCl *vs* P6 Eth $p < 0.001$***
Fig. 8B Latency to turn at 180° in negative geotaxis test over time	Two way ANOVA Tukey post-test	n = 37 in NaCl; n = 37 in Eth Females NaCl = 17 Females Eth = 18 Males NaCl = 20 Males Eth = 19	ANOVA F 1.366; $p = 0.2517$; ns Ages F 7.252; p < 0.0001**** Treatment F 0.7704; $p = 0.1288$; ns ANOVA F 0.1014; $p = 0.8279$; ns Time F 49.21; p < 0.0001**** Treatment F 12.87; p < 0.0001**** Tukey's P45 NaCl *vs* P45 Eth [0;10] p < 0.001*** P45 NaCl *vs* P45 Eth [10;20] $p < 0.01$** P45 NaCl *vs* P45 Eth [20;30] p < 0.001***
Fig. 8C Distance travelled in the entire compartment at P45 in three consecutive 10-min periods	Two way ANOVA Tukey post-test	n = 25 in NaCl; $n = 24$ in Eth Females NaCl = 12 Females Eth = 12 Males NaCl = 13 Males Eth = 12	
Fig. 8C Distance travelled in the entire compartment at P45 over 30 min	Unpaired t-test	n = 25 in NaCl; n = 24 in Eth Females NaCl = 12 Females Eth = 12	P45 NaCl *vs* P45 Eth [0;30] p < 0.0001****

(*continued on next page*)

Table 4 (*continued*)

Experiments	Test	n	p value
		Independents experiments	*p < 0.05; **p < 0.01; ***p < 0.001; ****p < 0.0001
		Males NaCl = 13 Males Eth = 12	
Fig. 8D Distance travelled in the central zone at P45 in three consecutive 10-min periods	Two way ANOVA Tukey post-test	n = 25 in NaCl; n = 24 in Eth Females NaCl = 12 Females Eth = 12 Males NaCl = 13 Males Eth = 12	ANOVA F 0.8366; p = 0.4107; ns Time F 27.57; p < 0.0001**** Treatment F 5.535; p < 0.001*** Tukey's P45 NaCl *vs* P45 Eth [0;10] p < 0.01**
Fig. 8D Distance travelled in the central zone at P45 over 30 min	Unpaired t-test	n = 25 in NaCl; n = 24 in Eth Females NaCl = 12 Females Eth = 12 Males NaCl = 13 Males Eth = 12	P45 NaCl *vs* P45 Eth [0;30] p < 0.05*
Fig. 8E Distance travelled in the peripheral zone at P45 in three consecutive 10-min periods	Two way ANOVA Tukey post-test	n = 25 in NaCl; n = 24 in Eth Females NaCl = 12 Females Eth = 12 Males NaCl = 13 Males Eth = 12	ANOVA F 0.2576; p = 0.6161; ns Time F 48.61; p < 0.0001**** Treatment F 13.85; p < 0.0001**** Tukey's P45 NaCl *vs* P45 Eth [0;10] p < 0.001*** P45 NaCl *vs* P45 Eth [10;20] p < 0.01*** P45 NaCl *vs* P45 Eth [20;30] p < 0.0001****
Fig. 8E Distance travelled in the peripheral zone at P45 over 30 min	Unpaired *t*-test	n = 25 in NaCl; n = 24 in Eth Females NaCl = 12 Females Eth = 12 Males NaCl = 13 Males Eth = 12	P45 NaCl *vs* P45 Eth [0;30] p < 0.0001****
Fig. 8G Immobility in the entire compartment at P45 in three consecutive 10-min periods	Two way ANOVA Tukey post-test	n = 25 in NaCl; n = 24 in Eth Females NaCl = 12 Females Eth = 12 Males NaCl = 13 Males Eth = 12	ANOVA F 0.1019; p = 0.8272; ns Time F 49.32; p < 0.0001**** Treatment F 12.74; p < 0.0001**** Tukey's P45 NaCl *vs* P45 Eth [0;10] p < 0.001*** P45 NaCl *vs* P45 Eth [10;20] p < 0.01** P45 NaCl *vs* P45 Eth [20;30] p < 0.0001****
Fig. 8G Immobility in the entire compartment at P45 over 30 min	Unpaired *t*-test	n = 25 in NaCl; n = 24 in Eth Females NaCl = 12 Females Eth = 12 Males NaCl = 13 Males Eth = 12	P45 NaCl *vs* P45 Eth [0;30] p < 0.0001****
Fig. 8H Immobility over 30 min at P45 in the	Two way ANOVA	n = 25 in NaCl; n = 24 in Eth Females NaCl = 12	ANOVA F 0.05429; p < 0.0001****

Table 4 (*continued*)

Experiments	Test	n	p value
		Independents experiments	*p < 0.05; **p < 0.01; ***p < 0.001; ****p < 0.0001
central and peripheral zone	Tukey post-test	Females Eth = 12 Males NaCl = 13 Males Eth = 12	Zone F 99.67; p < 0.0001**** Treatment F 0.07582; p < 0.0001**** Tukey's P45 NaCl CZ *vs* P45 NaCl PZ [0;30] p < 0.0001**** P45 Eth CZ *vs* P45 Eth PZ [0;30] p < 0.0001**** P45 NaCl PZ *vs* P45 Eth PZ [0;30] p < 0.0001****

3.2. PAE impairs the cortical vasculature but not the Olig2-vascular association

To evaluate the consequence of PAE on oligo-vascular interactions, double immunolabeling experiments targeting Olig2 and CD31 were performed in the developing cortex at three developmental stages, including E20, P2 and P15 (Fig. 3). As performed for human fetuses, 3D Imaris maps were built to validate and quantify oligo-vascular associations (Fig. 3A, B). Such an approach was required to exclude false-associated cells (Fig. 3B; arrowheads and Video S2). Two parameters were quantified: vascular organization and the percentage of Olig2-positive cells associated with microvessels (Fig. 3C-N).

Regarding vascular organization, at E20 and P2, radial microvessels (angle class [0–25[) represented the majority in the developing cortex (Fig. 3C-E and Fig. 3G-I). PAE significantly reduced and disorganized the cortical vasculature at both stages (Fig. 3E; Chi square NaCl E20 *vs.* Eth E20, df: 9.709, 3; *p = 0.0212 and Fig. 3I; Chi square NaCl P2 *vs.* Eth P2, df: 8.536, 3; *p = 0.0361). At P15, whereas radial microvessels remained the majority (Fig. 3K-M), no significant effect of PAE on the vascular organization of the cortex was found (Fig. 3M; Chi square NaCl P15 *vs.* Eth P15, df: 0.8597, 3; p = 0.8351). Concerning the oligo-vascular interactions, PAE did not modify the percentage of associated cells regardless of the stage and the cortical region considered (Fig. 3F, J, N).

3.3. PAE transiently altered the positioning of oligodendrocytes in the developing cortex

Because, on the one hand, the microvascular organization was impaired by PAE and, on the other hand, oligo-vascular association was preserved, we hypothesized that Olig2-positive cells could present positioning defects, as recently described for GABAergic interneurons (Léger et al., 2020b; Marguet et al., 2020). A time-course quantification of the density of Olig2-positive cells was performed at E20, P2 and P15 (Fig. 4). Under control conditions, Olig2-positive cells were present in deep (DCL) and superficial (SCL) cortical layers, and their density markedly increased from E20 to P2 in both regions (Fig. 4A, C, D; ****p < 0.0001). Afterward, a significant decrease occurred from P2 to P15 (Fig. 4C, D; ****p < 0.0001). No significant effect of PAE was observed on the density of Olig2-positive cells regardless of the stage considered (Fig. 4C, D; black bars). Quantification of the SCL/DCL ratio showed that under control conditions, a marked increase occurred between E20 and P2, reflecting the progressive invasion of the SCL by migrating oligodendrocytes (Fig. 4E; ****p < 0.0001). PAE significantly reduced SCL/

Table 5
Supplementary figures statistical analysis. The tests used, the number of independent experiments, the number of measures per experiment and *p* values are detailed for each experiments. Error bars in the graphs represent SEM.

Experiments	Test	n	p value
		Independents experiments	*p < 0.05; **p < 0.01; ***p < 0.001; ****p < 0.0001
Fig. S1A Weight tracking	Two way ANOVA Tukey post-test	n = 25 in NaCl; n = 24 in Eth	ANOVA Interaction F 0.07278; p = 0.0695; ns Ages F 96.85; p < 0.0001**** Treatment F 0.04493; p < 0.0011**
Fig. S1B Weight tracking in Females	Two way ANOVA Tukey post-test	n = 25 in NaCl; n = 24 in Eth Females NaCl = 12 Females Eth = 12 Males NaCl = 13 Males Eth = 12	ANOVA Interaction F 0.2042; p < 0.0001**** Ages F 98.32; p < 0.0001**** Treatment F 0.03235; p < 0.0058**
Fig. S1C Weight tracking in Males	Two way ANOVA Tukey post-test	n = 25 in NaCl; n = 24 in Eth Females NaCl = 12 Females Eth = 12 Males NaCl = 13 Males Eth = 12	ANOVA Interaction F 0.03507; p = 0.0532; ns Ages F 99.12; p < 0.0001**** Treatment F 0.04785; p < 0.0001****
Fig. S2A Distribution of olig2-positive cells density at E20	Chi-square test	n = 5 at least 3 slices analysed from 5 independent animals per treatment	Chi-square, df 0.1845, 2 p = 0.9119; ns
Fig. S2B Distribution of olig2-positive cells density at P2	Chi-square test	n = 5 at least 3 slices analysed from 5 independent animals per treatment	Chi-square, df 0.6670, 2 p = 0.7164; ns
Fig. S2C Distribution of olig2-positive cells density at P15	Chi-square test	n = 5 at least 3 slices analysed from 5 independent animals per treatment	Chi-square, df 0.2403, 2 p = 0.8868; ns
Fig. S2D Olig2-positive cells density in corpus callosum (CC)	Two way ANOVA Tukey post-test	n = 5 at least 3 slices analysed from 5 independent animals per treatment	ANOVA Interaction F 1.155; p = 0.7371; ns Ages F 46.33; p < 0.0001**** Treatment F 0.1407; p = 0.7861; ns Tukey's E20 NaCl *vs* P15 NaCl p < 0.05*
Fig. S2E Ratio Olig2-positive cells SCL *vs* DCL at E20	Unpaired *t*-test	n = 5 at least 3 slices analysed from 5 independent animals per treatment	NaCl *vs* Eth p = 0.8080; ns
Fig. S2F Ratio Olig2-positive cells SCL *vs* DCL at P15	Unpaired t-test	n = 5 at least 3 slices analysed from 5 independent	NaCl *vs* Eth p = 0.2843; ns

Table 5 (*continued*)

Experiments	Test	n	p value
		Independents experiments	*p < 0.05; **p < 0.01; ***p < 0.001; ****p < 0.0001
		animals per treatment	
Fig. S3A PDGFRα qRT–PCR on cortical extracts in Females	Two way ANOVA Tukey post-test	n = 16 animals per age and per treatment Males = 8 Females = 8	ANOVA Interaction F 0.4193; p = 0.2107; ns Ages F 91.77; p < 0.0001**** Treatment F 0.6680; p < 0.05* Tukey's E20 NaCl *vs* P2 NaCl p < 0.0001**** P2 NaCl *vs* P15 NaCl p < 0.0001**** E20 NaCl *vs* P15 NaCl p < 0.01**
Fig. S3B PDGFRα qRT–PCR on cortical extracts in Males	Two way ANOVA Tukey post-test	n = 16 animals per age and per treatment Males = 8 Females = 8	ANOVA Interaction F 0.2666; p = 0.6127; ns Ages F 89.74; p < 0.0001**** Treatment F 0.04027; p = 0.7008; ns Tukey's E20 NaCl *vs* P2 NaCl p < 0.0001**** P2 NaCl *vs* P15 NaCl p < 0.0001****
Fig. S3C CNPase qRT–PCR on cortical extracts in Females	Two way ANOVA Tukey post-test	n = 16 animals per age and per treatment Males = 8 Females = 8	ANOVA Interaction F 1.261; p = 0.1089; ns Ages F 86.04; p < 0.0001**** Treatment F 0.5934; p = 0.1456; ns Tukey's E20 NaCl *vs* P15 NaCl p < 0.0001**** P2 NaCl *vs* P15 NaCl p < 0.0001****
Fig. S3D CNPase qRT–PCR on cortical extracts in Males	Two way ANOVA Tukey post-test	n = 16 animals per age and per treatment Males = 8 Females = 8	ANOVA Interaction F 1.100; p = 0.4469; ns Ages F 73.55; p < 0.0001**** Treatment F 0.5546; p = 0.3680; ns Tukey's E20 NaCl *vs* P15 NaCl p < 0.0001**** P2 NaCl *vs* P15 NaCl p < 0.0001****
Fig. S3E MBP	Two way ANOVA	n = 16 animals per age and per treatment	ANOVA Interaction F 5.676; p < 0.05*

(*continued on next page*)

Table 5 (*continued*)

Experiments	Test	n	p value
		Independents experiments	*p < 0.05; **p < 0.01; ***p < 0.001; ****p < 0.0001
qRT–PCR on cortical extracts in Females	Tukey post-test	Males = 8 Females = 8	Ages F 62.39; p < 0.0001**** Treatment F 2.766; p < 0.05* Tukey's E20 NaCl *vs* P15 NaCl p < 0.0001**** P2 NaCl *vs* P15 NaCl p < 0.0001**** P15 NaCl *vs* P15 Eth p < 0.01**
Fig. S3F MBP qRT–PCR on cortical extracts in Males	Two way ANOVA Tukey post-test	n = 16 animals per age and per treatment Males = 8 Females = 8	ANOVA Interaction F 0.8260; p = 0.5474; ns Ages F 74.87; p < 0.0001**** Treatment F 0.3841; p = 0.4552; ns Tukey's E20 NaCl *vs* P15 NaCl p < 0.0001**** P2 NaCl *vs* P15 NaCl p < 0.0001****
Fig. S3G Olig2 qRT–PCR on cortical extracts in Females	Two way ANOVA Tukey post-test	n = 16 animals per age and per treatment Males = 8 Females = 8	ANOVA Interaction F 0.4205; p = 0.2810; ns Ages F 91.81; p < 0.0001**** Treatment F 0.05686; p = 0.5554; ns Tukey's E20 NaCl *vs* P2 NaCl p < 0.0001**** P2 NaCl *vs* P15 NaCl p < 0.0001****
Fig. S3H Olig2 qRT–PCR on cortical extracts in Males	Two way ANOVA Tukey post-test	n = 16 animals per age and per treatment Males = 8 Females = 8	ANOVA Interaction F 0.1477; p = 0.0607; ns Ages F 85.54; p < 0.0001**** Treatment F 1.934; p < 0.01** Tukey's E20 NaCl *vs* P2 NaCl p < 0.0001**** P2 NaCl *vs* P15 NaCl p < 0.0001**** P2 NaCl *vs* P2 Eth p < 0.01**
Fig. S4A Western blot PDGFα on cortical extracts at E20	Two way ANOVA Tukey post-test	n = 16 animals per age and per treatment Males = 8 Females = 8	ANOVA Interaction F 0.0003; p = 0.9926; ns Sexes F 1.342; p = 0.5465; ns Treatment F

Table 5 (*continued*)

Experiments	Test	n	p value
		Independents experiments	*p < 0.05; **p < 0.01; ***p < 0.001; ****p < 0.0001
Fig. S4B Western blot PDGFα on cortical extracts at P2	Two way ANOVA Tukey post-test	n = 16 animals per age and per treatment Males = 8 Females = 8	9.226; p = 0.1216; ns ANOVA Interaction F 9.615; p = 0.1141; ns Sexes F 4.287; p = 0.2844; ns Treatment F 0.2702; p = 0.7858; ns
Fig. S4C Western blot PDGFα on cortical extracts at P15	Two way ANOVA Tukey post-test	n = 16 animals per age and per treatment Males = 8 Females = 8	ANOVA Interaction F 0.4724; p = 0.7210; ns Sexes F 0.09618; p = 0.8718; ns Treatment F 1.518; p = 0.5231; ns
Fig. S4D Western blot CNPase on cortical extracts at E20	Two way ANOVA Tukey post-test	n = 16 animals per age and per treatment Males = 8 Females = 8	ANOVA Interaction F 0.1520; p = 0.8242; ns Sexes F 3.724; p = 0.2766; ns Treatment F 16.17; p < 0.05*
Fig. S4E Western blot CNPase on cortical extracts at P2	Two way ANOVA Tukey post-test	n = 16 animals per age and per treatment Males = 8 Females = 8	ANOVA Interaction F 2^{e-005}; p = 0.9979; ns Sexes F 0.2077; p = 0.7914; ns Treatment F 24.25; p < 0.01**
Fig. S4F Western blot CNPase on cortical extracts at P15	Two way ANOVA Tukey post-test	n = 16 animals per age and per treatment Males = 8 Females = 8	ANOVA Interaction F 0.02871; p = 0.9221; ns Sexes F 1.100; p = 0.5462; ns Treatment F 12.49; p < 0.05*
Fig. S4G Western blot Olig2 on cortical extracts at E20	Two way ANOVA Tukey post-test	n = 16 animals per age and per treatment Males = 8 Females = 8	ANOVA Interaction F 0.007199; p = 0.9607; ns Sexes F 5.868; p = 0.1658; ns Treatment F 5.416; p = 0.1825; ns
Fig. S4H Western blot Olig2 on cortical extracts at P2	Two way ANOVA Tukey post-test	n = 16 animals per age and per treatment Males = 8 Females = 8	ANOVA Interaction F 0.2240; p = 0.8086; ns Sexes F 0.6667; p = 0.6765; ns Treatment F 1.844; p = 0.4890; ns
Fig. S4I Western blot Olig2 on cortical extracts at P15	Two way ANOVA Tukey post-test	n = 16 animals per age and per treatment Males = 8 Females = 8	ANOVA Interaction F 2.079; p = 0.4452; ns Sexes F 0.5403; p = 0.6960; ns Treatment F

(*continued on next page*)

Table 5 (*continued*)

Experiments	Test	n	p value
		Independents experiments	*p < 0.05; **p < 0.01; ***p < 0.001; ****p < 0.0001
Fig. S4 J Western blot MBP on cortical extracts at P15	Two way ANOVA Tukey post-test	n = 16 animals per age and per treatment Males = 8 Females = 8	0.3442; p = 0.7551; ns ANOVA Interaction F 1.476; p = 0.4459; ns Sexes F 1.289; p = 0.4760; ns Treatment F 26.90; p < 0.01** Tukey's P15 NaCl Females *vs* P15 Eth Females p < 0.05*
Fig. S5C MBP bundles density in the striatum at P15	Unpaired t-test	n = 5 at least 2 slices analysed from 5 independent animals per treatment	NaCl *vs* Eth p < 0.01**
Fig. S5D MBP bundles aera in the striatum at P15	Unpaired t-test	n = 5 at least 2 slices analysed from 5 independent animals per treatment	NaCl *vs* Eth p < 0.05*
Fig. S5E Distribution of MBP bundle areas at P15	Chi-square test	n = 5 at least 2 slices analysed from 5 independent animals per treatment	Chi-square, df 0.7006, 6 p = 0.9945; ns
Fig. S6A Western blot MBP on cortical extracts at P45	Unpaired t-test	n = 16 animals per age and per treatment Males = 8 Females = 8	NaCl *vs* Eth p = 0.8722; ns
Fig. S6B Western blot MBP on cortical extracts at P45	Two way ANOVA Tukey post-test	n = 16 animals per age and per treatment Males = 8 Females = 8	ANOVA Interaction F 3.029; p = 0.3630; ns Sexe F 1.184; p = 0.5677; ns Treatment F 0.2588; p = 0.7889; ns
Fig. S6C Western blot MBP on corpus callosum extracts at P45	Unpaired t-test	n = 8 animals per age and per treatment Males = 4 Females = 4	NaCl *vs* Eth p = 0.2401; ns
Fig. S6D Western blot MBP on corpus callosum extracts at P45	Two way ANOVA Tukey post-test	n = 8 animals per age and per treatment Males = 4 Females = 4	ANOVA Interaction F 0.4496; p = 0.8090; ns Sexe F 1.434; p = 0.6669; ns Treatment F 9.757; p = 0.2721; ns
Fig. S6G MBP bundles density at P45	Unpaired t-test	n = 16 animals per age and per treatment Males = 8 Females = 8	NaCl *vs* Eth p = 0.9345; ns
Fig. S6H MBP bundles area at P45	Unpaired *t*-test	n = 16 animals per age and per treatment	NaCl *vs* Eth p = 0.8946; ns

Table 5 (*continued*)

Experiments	Test	n	p value
		Independents experiments	*p < 0.05; **p < 0.01; ***p < 0.001; ****p < 0.0001
Fig. S6I Distribution of MBP bundle areas at P45	Chi-square test	Males = 8 Females = 8 n = 5 at least 2 slices analysed from 5 independent animals per treatment	Chi-square, df 0.5808, 6 p = 0.9967; ns
Fig. S7A Latency to turn in the righting reflex test over time in Females	Two way ANOVA Tukey post-test	n = 37 in NaCl; n = 37 in Eth Females NaCl = 17 Females Eth = 18 Males NaCl = 20 Males Eth = 19	ANOVA Interaction F 12.98; p < 0.0001**** Ages F 23.86; p < 0.0001**** Treatment F 0.2173; p = 0.4094; ns Tukey's P2 NaCl Females *vs* P2 Eth Females p < 0.01** P6 NaCl Females *vs* P6 Eth Females p < 0.05*
Fig. S7B Latency to turn in the righting reflex test over time in Males	Two way ANOVA Tukey post-test	n = 37 in NaCl; n = 37 in Eth Females NaCl = 17 Females Eth = 18 Males NaCl = 20 Males Eth = 19	ANOVA Interaction F 6.634; p < 0.001*** Ages F 31.56; p < 0.0001**** Treatment F 0.02647; p = 0.7511; ns Tukey's P2 NaCl Males *vs* P2 Eth Males p < 0.01**
Fig. S7C Latency to turn at 180° in negative geotaxis test over time in Females	Two way ANOVA Tukey post-test	n = 37 in NaCl; n = 37 in Eth Females NaCl = 17 Females Eth = 18 Males NaCl = 20 Males Eth = 19	ANOVA Interaction F 2.311; p = 0.3707; ns Ages F 8.6; p < 0.05* Treatment F 0.09161; p = 0.7237; ns
Fig. S7D Latency to turn at 180° in negative geotaxis test over time in Males	Two way ANOVA Tukey post-test	n = 37 in NaCl; n = 37 in Eth Females NaCl = 17 Females Eth = 18 Males NaCl = 20 Males Eth = 19	ANOVA Interaction F 1.337; p = 0.5579; ns Ages F 9.388; p < 0.01** Treatment F 1.147; p = 0.1838; ns
Fig. S8A Distance travelled in the entire compartment at P15 in three consecutive 10-min periods	Two way ANOVA Tukey post-test	n = 25 in NaCl; n = 24 in Eth Females NaCl = 12 Females Eth = 12 Males NaCl = 13 Males Eth = 12	ANOVA Interaction F 0.9559; p = 0.5032; ns Time F 1.036; p = 0.4752; ns Treatment F 0.3930; p = 0.4525; ns
Fig. S8A Distance travelled in the entire compartment at P15 over 30 min	Unpaired t-test	n = 25 in NaCl; n = 24 in Eth Females NaCl = 12 Females Eth = 12	P15 NaCl *vs* P15 Eth [0;30]; p = 0.6181; ns

(*continued on next page*)

Table 5 (*continued*)

Experiments	Test	n	p value
		Independents experiments	*p < 0.05; **p < 0.01; ***p < 0.001; ****p < 0.0001
Fig. S8B Distance travelled in the entire compartment at P15 in three consecutive 10-min periods in Females	Two way ANOVA Tukey post-test	Males NaCl = 13 Males Eth = 12 n = 25 in NaCl; n = 24 in Eth Females NaCl = 12 Females Eth = 12 Males NaCl = 13 Males Eth = 12	ANOVA Interaction F 0.5178; p = 0.8421; ns Time F 0.2977; p = 0.9058; ns Treatment F 0.0008; p = 0.9815; ns
Fig. S8B Distance travelled in the entire compartment at P15 over 30 min in Females	Unpaired t-test	n = 25 in NaCl; n = 24 in Eth Females NaCl = 12 Females Eth = 12 Males NaCl = 13 Males Eth = 12	P15 NaCl *vs* P15 Eth [0;30]; p = 0.9880; ns
Fig. S8C Distance travelled in the entire compartment at P15 in three consecutive 10-min periods in Males	Two way ANOVA Tukey post-test	n = 25 in NaCl; n = 24 in Eth Females NaCl = 12 Females Eth = 12 Males NaCl = 13 Males Eth = 12	ANOVA Interaction F 2.556; p = 0.3876; ns Time F 5.312; p = 0.1435; ns Treatment F 0.3875; p = 0.5911; ns
Fig. S8C Distance travelled in the entire compartment at P15 over 30 min in Males	Unpaired t-test	n = 25 in NaCl; n = 24 in Eth Females NaCl = 12 Females Eth = 12 Males NaCl = 13 Males Eth = 12	P15 NaCl *vs* P15 Eth [0;30]; p = 0.7254; ns
Fig. S8D Immobility in the entire compartment at P15 in three consecutive 10-min periods	Two way ANOVA Tukey post-test	n = 25 in NaCl; n = 24 in Eth Females NaCl = 12 Females Eth = 12 Males NaCl = 13 Males Eth = 12	ANOVA Interactions F 0.7857; p = 0.5684; ns Time F 1.232; p = 0.4131; ns Treatment F 0.3417; p = 0.4836; ns
Fig. S8D Immobility in the entire compartment at P15 over 30 min	Unpaired t-test	n = 25 in NaCl; n = 24 in Eth Females NaCl = 12 Females Eth = 12 Males NaCl = 13 Males Eth = 12	P15 NaCl *vs* P15 Eth [0;30] p = 0.6407; ns
Fig. S8E Immobility in the entire compartment at P15 in three consecutive 10-min periods in Females	Two way ANOVA Tukey post-test	n = 25 in NaCl; n = 24 in Eth Females NaCl = 12 Females Eth = 12 Males NaCl = 13 Males Eth = 12	ANOVA Interactions F 0.7385; p = 0.7819; ns Time F 0.1376; p = 0.9551; ns Treatment F 0.4325; p = 0.5925; ns
Fig. S8E Immobility in the entire compartment at P15 over 30 min in Females	Unpaired t-test	n = 25 in NaCl; n = 24 in Eth Females NaCl = 12 Females Eth = 12 Males NaCl = 13 Males Eth = 12	P15 NaCl *vs* P15 Eth [0;30] p = 0.7238; ns
Fig. S8F Immobility in the entire compartment at P15 in three consecutive 10-min periods in Males	Two way ANOVA Tukey post-test	n = 25 in NaCl; n = 24 in Eth Females NaCl = 12 Females Eth = 12 Males NaCl = 13 Males Eth = 12	ANOVA Interactions F 2.0; p = 0.4775; ns Time F 5.456; p = 0.1380; ns Treatment F 0.2101; p = 0.6932; ns
Fig. S8F Immobility in the entire compartment at P15 over 30 min in Males	Unpaired t-test	n = 25 in NaCl; n = 24 in Eth Females NaCl = 12 Females Eth = 12 Males NaCl = 13 Males Eth = 12	P15 NaCl *vs* P15 Eth [0;30] p = 0.7942; ns
Fig. S8G Time spent in the central zone at P15 in three consecutive 10-min periods	Two way ANOVA Tukey post-test	n = 25 in NaCl; n = 24 in Eth Females NaCl = 12 Females Eth = 12 Males NaCl = 13 Males Eth = 12	ANOVA Interaction F 0.7809; p = 0.5334; ns Time F 12.02; p < 0.001*** Treatment F 0.01559; p = 0.8741; ns
Fig. S8G Time spent in the central zone at P15 over 30 min	Unpaired t-test	n = 25 in NaCl; n = 24 in Eth Females NaCl = 12 Females Eth = 12 Males NaCl = 13 Males Eth = 12	P15 NaCl *vs* P15 Eth [0;30] p = 0.9003; ns
Fig. S8H Time spent in the central zone at P15 in three consecutive 10-min periods in Females	Two way ANOVA Tukey post-test	n = 25 in NaCl; n = 24 in Eth Females NaCl = 12 Females Eth = 12 Males NaCl = 13 Males Eth = 12	ANOVA Interaction F 2.331; p = 0.3926; ns Time F 11.46; p < 0.05* Treatment F 5.116; p < 0.05*
Fig. S8H Time spent in the central zone at P15 over 30 min in Females	Unpaired t-test	n = 25 in NaCl; n = 24 in Eth Females NaCl = 12 Females Eth = 12 Males NaCl = 13 Males Eth = 12	P15 NaCl *vs* P15 Eth [0;30] p = 0.0881; ns
Fig. S8I Time spent in the central zone at P15 in three consecutive 10-min periods in Males	Two way ANOVA Tukey post-test	n = 25 in NaCl; n = 24 in Eth Females NaCl = 12 Females Eth = 12 Males NaCl = 13 Males Eth = 12	ANOVA Interactions F 2.412; p = 0.3644; ns Time F 14.00; p < 0.01** Treatment F 1.987; p = 0.1982; ns
Fig. S8I Time spent in the central zone at P15 over 30 min in Males	Unpaired t-test	n = 25 in NaCl; n = 24 in Eth Females NaCl = 12 Females Eth = 12 Males NaCl = 13 Males Eth = 12	P15 NaCl *vs* P15 Eth [0;30] p = 0.3343; ns
Fig. S9A Distance travelled in the entire compartment at P45 in three consecutive 10-min periods in Females	Two way ANOVA Tukey post-test	n = 25 in NaCl; n = 24 in Eth Females NaCl = 12 Females Eth = 12 Males NaCl = 13 Males Eth = 12	ANOVA Interaction F 0.1131; p = 0.9200; ns Time F 45.45; p < 0.0001**** Treatment F 9.742; p < 0.001*** Tukey's P45 NaCl *vs* P45 Eth [0;10] p < 0.05*
Fig. S9A Distance travelled in the entire compartment at P45 over 30 min in Females	Unpaired t-test	n = 25 in NaCl; n = 24 in Eth Females NaCl = 12 Females Eth = 12 Males NaCl = 13 Males Eth = 12	P15 NaCl *vs* P15 Eth [0;30] p < 0.05*
Fig. S9B Distance travelled in	Two way ANOVA	n = 25 in NaCl; n = 24 in Eth	ANOVA Interaction F

(*continued on next page*)

Table 5 (*continued*)

Experiments	Test	n	p value
		Independents experiments	*p < 0.05; **p < 0.01; ***p < 0.001; ****p < 0.0001
the entire compartment at P45 in three consecutive 10-min periods in Males	Tukey post-test	Females NaCl = 12 Females Eth = 12 Males NaCl = 13 Males Eth = 12	0.1656; p = 0.8297; ns Time F 53.00; p < 0.0001**** Treatment F 16.29; p < 0.0001**** Tukey's P45 NaCl *vs* P45 Eth [0;10] p < 0.01** P45 NaCl *vs* P45 Eth [10;20] p < 0.01** P45 NaCl *vs* P45 Eth [20;30] p < 0.001***
Fig. S9B Distance travelled in the entire compartment at P45 over 30 min in Males	Unpaired t-test	n = 25 in NaCl; n = 24 in Eth Females NaCl = 12 Females Eth = 12 Males NaCl = 13 Males Eth = 12	P15 NaCl *vs* P15 Eth [0;30] p < 0.001***
Fig. S9C Immobility in the entire compartment at P45 in three consecutive 10-min periods in Females	Two way ANOVA Tukey post-test	n = 25 in NaCl; n = 24 in Eth Females NaCl = 12 Females Eth = 12 Males NaCl = 13 Males Eth = 12	ANOVA Interactions F 0.08662; p = 0.9394; ns Time F 44.76; p < 0.0001**** Treatment F 9.509; p < 0.001***
Fig. S9C Immobility in the entire compartment at P45 over 30 min in Females	Unpaired t-test	n = 25 in NaCl; n = 24 in Eth Females NaCl = 12 Females Eth = 12 Males NaCl = 13 Males Eth = 12	P15 NaCl *vs* P15 Eth [0;30] p < 0.05*
Fig. S9D Immobility in the entire compartment at P45 in three consecutive 10-min periods in Males	Two way ANOVA Tukey post-test	n = 25 in NaCl; n = 24 in Eth Females NaCl = 12 Females Eth = 12 Males NaCl = 13 Males Eth = 12	ANOVA Interaction F 0.2050; p = 0.7875; ns Time F 54.01; p < 0.0001**** Treatment F 16.33; p < 0.0001**** Tukey's P45 NaCl *vs* P45 Eth [0;10] p < 0.01** P45 NaCl *vs* P45 Eth [10;20] p < 0.01** P45 NaCl *vs* P45 Eth [20;30] p < 0.001***
Fig. S9D Immobility in the entire compartment at P45 over 30 min in Males	Unpaired t-test	n = 25 in NaCl; n = 24 in Eth Females NaCl = 12 Females Eth = 12 Males NaCl = 13 Males Eth = 12	P15 NaCl *vs* P15 Eth [0;30] p < 0.001***
Fig. S9E Time spent in the central zone at P45 in three consecutive 10-min periods	Two way ANOVA Tukey post-test	n = 25 in NaCl; n = 24 in Eth Females NaCl = 12 Females Eth = 12 Males NaCl = 13 Males Eth = 12	ANOVA Interactions F 0.9409; p = 0.5118; ns Time F 0.3515; p = 0.7781; ns Treatment F 0.1230; p = 0.6755; ns
Fig. S9E Time spent in the central zone at P45 over 30 min	Unpaired t-test	n = 25 in NaCl; n = 24 in Eth Females NaCl = 12 Females Eth = 12 Males NaCl = 13 Males Eth = 12	P45 NaCl *vs* P45 Eth [0;30] p = 0.7584; ns
Fig. S9F Time spent in the central zone at P45 in three consecutive 10-min periods in Females	Two way ANOVA Tukey post-test	n = 25 in NaCl; n = 24 in Eth Females NaCl = 12 Females Eth = 12 Males NaCl = 13 Males Eth = 12	ANOVA Interactions F 0.6145; p = 0.8102; ns Time F 3.321; p = 0.3257; ns Treatment F 0.001637; p = 0.9733; ns
Fig. S9F Time spent in the central zone at P45 over 30 min in Females	Unpaired t-test	n = 25 in NaCl; n = 24 in Eth Females NaCl = 12 Females Eth = 12 Males NaCl = 13 Males Eth = 12	P45 NaCl *vs* P45 Eth [0;30] p = 0.9815; ns
Fig. S9G Time spent in the central zone at P45 in three consecutive 10-min periods in Males	Two way ANOVA Tukey post-test	n = 25 in NaCl; n = 24 in Eth Females NaCl = 12 Females Eth = 12 Males NaCl = 13 Males Eth = 12	ANOVA Interactions F 1.335; p = 0.6192; ns Time F 2.766; p = 0.3730; ns Treatment F 0.3924; p = 0.5959; ns
Fig. S9G Time spent in the central zone at P45 over 30 min in Males	Unpaired t-test	n = 25 in NaCl; n = 24 in Eth Females NaCl = 12 Females Eth = 12 Males NaCl = 13 Males Eth = 12	P45 NaCl *vs* P45 Eth [0;30] p = 0.6839; ns

DCL ratio at P2 (Fig. 4E-G; *p < 0.05). Although observed at P15, the SCL/DCL imbalance was lower and no more significant (Fig. S2F). A similar analysis was performed in the corpus callosum and did not show a significant effect of PAE on the density of Olig2-positive cells (Fig. S2D). Altogether, these data indicate that Olig2-positive cells progressively invade the neocortex in a regionalized and timeline-dependent manner. During the postnatal period, PAE impaired the balance of Olig2-positive cells positioned in the deep and superficial cortical layers.

3.4. PAE altered the expression of differentiation markers of the oligodendrocyte lineage in the developing cortex

According to clinical data, consumption of alcohol during pregnancy can lead to white matter impairments (Mattson et al., 2011). Because studies performed in nonhuman primates supported the stage-dependent vulnerability of oligodendrocytes to alcohol (Creeley et al., 2013), we studied the effect of PAE on the expression of differentiation markers of the oligodendrocyte lineage at stages where oligo-vascular defects were observed using RT–PCR and western blot (E20-P15; Fig. 5). PDGFRα served as a marker of progenitors (OPCs) and pre-oligodendrocytes (pre-OLs), CNPase was used as a transition marker from pre-OLs to immature oligodendrocytes, MBP was used as a marker of mature oligodendrocytes, and Olig2 was used as a full lineage marker (Fig. 1C). Under control conditions, PDGFRα mRNA expression

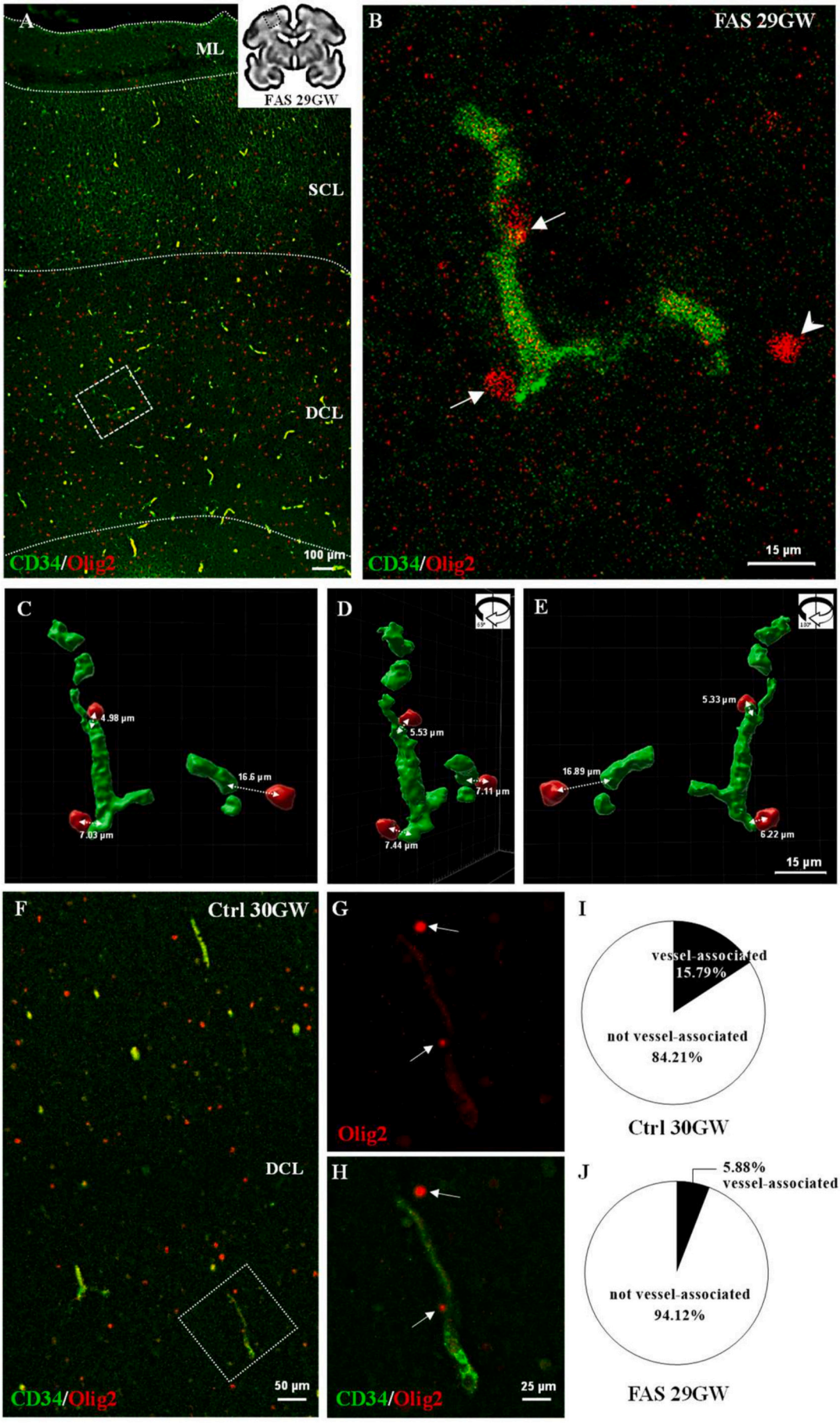

(caption on next page)

Fig. 2. Oligovascular interactions in the human fetal cortex. A. Immunohistochemistry experiments targeting Olig2 and CD34 in human neocortices from a FAS fetus at gestational week 29 (29GW). B. Focus on one vessel (x40), presenting associated (arrows) and nonassociated (arrowheads) Olig2-positive cells. C-E. 3D IMARIS reconstruction of *Z*-stacks acquired from B. The 3D map is visualized under three different angles (0°; 65°; 180°). Morphometric analysis consisted of measuring the distance between Olig2-positive nuclei and the center of the microvessel (dotted bare line). F—H. Visualization of oligo-vascular interactions in the control fetus (Ctrl) at 30 GW at low (F) and high (G, H) magnification. I, J. Quantification of the number of vessel-associated Olig2-positive cells in the deep cortex of control (I) and FAS (J) fetuses.

significantly increased from E20 to P2 and subsequently decreased to P15 (Fig. 5A; ****p < 0.0001). CNPase and MBP expression progressively increased from E20 to P15 (Fig. 5B, C; ****p < 0.0001), whereas a bell-shaped profile of mRNA Olig2 expression was observed (Fig. 5D). PAE differentially impacted the expression of these markers. Specifically, no effect on PDGFRα and Olig2 mRNA expression was noted (Fig. 5A, D; black bars), and a decrease in CNPase expression was quantified at P15 (Fig. 5B; black bars). Finally, a reduction in MBP expression was first detected at P2 and became significant at P15 (Fig. 5C; black bars; ##$p < 0.01$). RT–PCR quantifications were systematically performed considering females and males (Fig. S3). While the data were, most of the time, similar between the two sexes, one result showed sex-dependent specificity. Indeed, the inhibitory effect of PAE on MBP expression was more pronounced in females (Fig. S3E; ##p < 0.01).

Western blot experiments revealed that PAE did not modify the expression of PDGFRα or Olig2 (Fig. 5E, F, I). CNPase protein levels were reduced by PAE at all stages E20 ($p < 0.05$), P2 ($p < 0.01$) and P15 (Fig. 5E, G). MBP was not detected by western blot at E20 and P2, whereas PAE induced a marked decrease in MBP protein levels at P15 (Fig. 5E, H; **p < 0.01). As performed for RT–PCR experiments, western blot data were expressed considering females and males at E20, P2 and P15 (Fig. S4). While the results were very similar between the sexes, the inhibitory effect of PAE on MBP protein levels was more pronounced in females (Fig. S4J). Altogether, these data indicate that PAE differentially impaired the expression of maturation markers of oligodendrocytes in the developing cortex, affecting CNPase and MBP, which are indicators of immature and mature oligodendrocytes, respectively.

3.5. PAE inverted the distribution profiles of CNPase and MBP in the developing cortex

Whereas RT–PCR and western blot experiments provide data regarding expression levels, the use of tissue homogenates did not make it possible to determine whether specific cortical areas were affected. To research evidence of alcohol-induced impairments of oligodendrocyte maturation in the developing cortex, we established the distribution profiles of CNPase and MBP immunoreactivities at P15 (Fig. 6). In the control condition, linescan acquisitions showed that CNPase immunoreactivity was distributed in all cortical layers (Fig. 6A, C). Quantification of the areas under the curve (AUC) indicated that the CNPase-related signal was higher in layers V and VI (Fig. 6D; *$p < 0.05$). Similarly, the cortical distribution of the MBP-like signal was determined at P15 (Fig. 6E-H). In control mice, the MBP-associated signal was maximal in layer VI and progressively decreased up to layer I (Fig. 6G). PAE induced a significant decrease in the MBP-integrated signal in cortical layer VI (Fig. 6H; *p < 0.05). Interestingly, the comparative analysis of CNPase and MBP profiles indicated that, in the control condition, linescan curves intersected at the level of layer V (Fig. 6I). In contrast, in the PAE group, CNPase and MBP profiles never intersected (Fig. 6J). Accordingly, the MBP/CNPase ratio was significantly reduced in layer VI after PAE (Fig. 6K; **$p < 0.01$). Altogether, these data indicate that the effects of PAE quantified by RT–PCR and western blot reflected impairment of the maturation profiles of oligodendrocytes along cortical layers.

3.6. PAE impaired axonal myelination of efferent cortical axons

Axons from cortical pyramidal cells constitute efferent projections and belong to interhemispheric and corticofugal pathways (Usrey and Sherman, 2019). To determine whether the modification of the CNPase/MBP ratio evidenced at P15 in the developing cortex was associated with alteration of corticofugal pathways, we explored the effects of PAE on striatal myelinated (MBP-positive) bundles at P15 (Fig. S5A, B). However, PAE induced an increase in MBP-positive bundle density (Fig. S5C; *p < 0.01) as well as a significant decrease in their areas (Fig. S5D; **p < 0.01). Accordingly, the distribution of MBP-positive bundles showed that PAE increased the proportion of small bundles (Fig. S5E). Surprisingly, the effects of PAE evidenced at P15 were not retrieved at P45 (adult mice) for both MBP expression (Fig. S6A-D) and striatal bundles (Fig. S6E-I). Because efferent cortical fibers run through the corpus callosum, we performed electronic microscopy acquisitions at P15 to quantify the impact of PAE on myelinated axons (Fig. 7). Compared to the control condition, PAE induced a decrease in the density of myelinated axons (Fig. 7A, C, E; *$p < 0.05$). This effect was associated with a marked reduction in the thickness of the myelin sheath (Fig. 7B, D, F; ***$p < 0.001$). Furthermore, measurement of axonal section areas indicated that PAE increased the percentage of small axons (Fig. 7G). Altogether, these data indicate that the decrease in MBP expression after PAE is associated with both neuronal (reduced axon density) and oligodendrocyte (reduced myelin sheath) impairments.

3.7. PAE induced neonatal sensorimotor disabilities and persistent locomotor disorders

In several human pathologies and animal models, impaired myelination is associated with motor disabilities, although not exclusively (Niu et al., 2021; Ueda et al., 2018). To investigate whether PAE oligovascular impairments identified in the perinatal period are correlated with sensorimotor disorders, behavioral tests were conducted in PAE-exposed neonates from P2 to P8 (Fig. 8A, B; Fig. S7) as well as at P15 (Fig. S8) and P45 (Fig. 8C-H and Fig. S9). In control neonates, the righting reflex test showed that latency to turn from the supine position to a normal prone position regularly decreased from P2 to P8 (Fig. 8A; black curve). In contrast, PAE neonates presented at P2 a tonic profile characterized by a propensity to rapidly return in the prone position (Fig. 8A; ****p < 0.001). However, no evolution of the latency to turn was measured until P6 (Fig. 8A; dotted curve). At P6, PAE neonates were substantially less rapid to turn than control neonates (Fig. 8A; ***p < 0.01). While observed in both females and males, the effect of PAE was more pronounced in females (Fig. S7A, B). In the negative geotaxis test, no effect of PAE was quantified regardless of the stage and sex considered (Fig. 8B; Fig. S7C, D). To assess the long-term motor effects of PAE, locomotor activity was analysed at P15 (Fig. S8) and P45 using an open field (Fig. 8C-H; Fig. S9). At P15, PAE had no significant effect on the locomotor activity of either females or males measured in the entire compartment or in peripheral and central areas (Fig. S8). Furthermore, PAE did not impair the time spent in the central zone (Fig. S8G-I). At P45 (adult stage), PAE induced a marked reduction in the distance travelled by mice (Fig. 8C, F; red line tracking; ****p < 0.001 after 30 min). A similar effect was found when central and peripheral regions were separately analysed (Fig. 8D, E). To determine whether the decrease in the travelled distance resulted from a slower travel speed or longer periods of immobility, mobility maps were analysed (Fig. 8F; false color

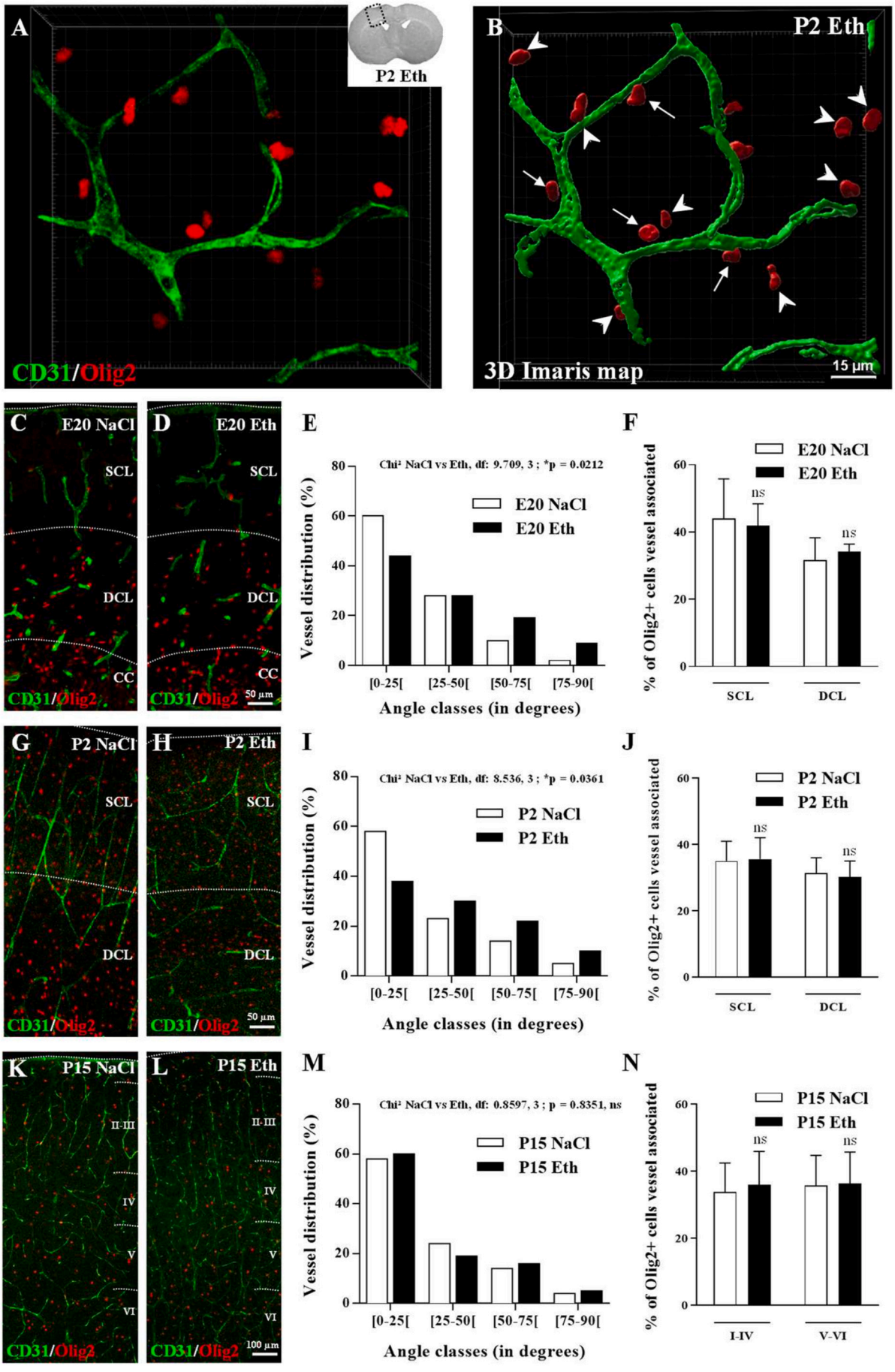

(caption on next page)

Fig. 3. Effect of PAE on oligo-vascular interactions in the neocortex of mouse neonates. A. Visualization by double immunolabeling of Olig2-positive cells and microvessels (CD31) in the developing cortex at P2 (A). B. 3D map reconstruction of the Z-stack acquisition shown in A. Cells interacting with microvessels (distance <10 μm) are indicated by arrows. Olig2-positive cells at the distance of microvessels are indicated by arrowheads. A video is provided as a supplementary file to clearly objectivize cell distances. C, D. Immunohistochemistry experiments visualizing the association of Olig2-positive cells with radial microvessels in control (C) and alcohol-exposed (D) cortices at E20. E. Distribution of microvessel orientation (angle classes) in the developing cortex of control (white bars) and alcohol-exposed (black bars) mice at E20. Statistical analysis was performed using the $\chi 2$ test. F. Percentage of Olig2-positive cells associated with microvessels in the developing superficial (SCL) and deep (DCL) cortical layers of control (white bars) and alcohol-exposed (black bars) mice at E20. Statistical analysis was performed using two-way ANOVA. G, H. Immunohistochemistry experiments visualizing the association of Olig2-positive cells with radial microvessels in control (G) and alcohol-exposed (H) cortices at P2. I. Distribution of microvessel orientation (angle classes) in the developing cortex of control (white bars) and alcohol-exposed (black bars) mice at P2. Statistical analysis was performed using the $\chi 2$ test. J. Percentage of Olig2-positive cells associated with microvessels in the developing superficial (SCL) and deep (DCL) cortical layers of control (white bars) and alcohol-exposed (black bars) mice at P2. Statistical analysis was performed using ANOVA. K, L. Immunohistochemistry experiments visualizing the association of Olig2-positive cells with radial microvessels in control (G) and alcohol-exposed (H) cortices at P15. M. Distribution of microvessel orientation (angle classes) in the developing cortex of control (white bars) and alcohol-exposed (black bars) mice at P15. Statistical analysis was performed using the $\chi 2$ test. N. Percentage of Olig2-positive cells associated with microvessels in cortical layers I-IV and V-VI of control (white bars) and alcohol-exposed (black bars) mice at P15. Statistical analysis was performed using ANOVA. CC: corpus callosum; DCL: deep cortical layers; SCL: superficial cortical layers; Eth: Ethanol, I-VI: cortical layers I to VI.

scale). PAE induced a significant increase in the period of immobility (Fig. 8G; ****$p < 0.001$ after 30 min). These periods of immobility were essentially observed in the peripheral part of the open field (Fig. 8H). The effects of PAE on locomotor activity were similar between females and males (Fig. S9 A-D; *$p < 0.05$ and ***$p < 0.001$, respectively).

4. Discussion

The present study revealed the following highlights: *i)* as shown for cortical interneurons, oligodendrocytes invading cortical layers are associated with radial microvessels; *ii)* the vessel association of Olig2-positive cells is found in humans and mice; *iii)* despite vascular disorganization induced by PAE, the vessel association of Olig2-positive cells persisted; *iv)* PAE transiently impaired the distribution of Olig2-positive cells between deep and superficial cortical layers; *v)* the effect of PAE on the cortical positioning of Olig2-positive cells was associated with dysregulation of the expression of differentiation markers of oligodendrocytes; and *vi)* PAE induced myelination deficits associated with long-term behavioral disabilities (Fig. 9).

It is well established in the literature that alcohol consumption during pregnancy can lead to neurodevelopmental disabilities (Chasnoff et al., 2015; Riley et al., 2011) and, in particular, to white matter defects (Donald et al., 2015; Lebel et al., 2011; Riley et al., 1995). Recently, several studies have shown that PAE delays the maturation of oligodendrocytes (Darbinian et al., 2021). For example, it has been described that prenatal alcohol exposure is associated with delayed oligodendrocyte maturation in the human fetal brain. Nevertheless, the processes involved in these developmental defects are far from understood. In the last decade, major discoveries have been made regarding modalities of tangential migration of immature oligodendrocytes (Tsai et al., 2016). Indeed, migrating OPCs generated in ganglionic eminences reach the developing corpus callosum using periventricular tangential microvessels as guides (Tsai et al., 2016). In addition, numerous oligodendrocytes invade and populate the cortical layers, although their migration modalities remain unclear (Choe et al., 2014). We recently demonstrated in both human and animal models that PAE disorganizes the radial organization of cortical microvessels (Jégou et al., 2012; Lecuyer et al., 2017; Li et al., 2021). Regarding our recent data and those from Tsai and coworkers, it was tempting to hypothesize the existence of a vascular link in the deleterious effects of PAE on oligodendrocyte differentiation.

4.1. Radial microvessels support cortical oligodendrocytes

During brain development, immature GABAergic interneurons and oligodendrocytes share similarities starting with their migration (Luhmann et al., 2015; Paredes et al., 2018; Segara et al., 2019;). In contrast to the large majority of cortical glutamatergic neurons, most cortical GABAergic interneurons are generated in ganglionic eminences and reach the neocortex using a vessel-associated tangential migration mode (Luhmann et al., 2015; Won et al., 2013). In particular, migrating interneurons arriving tangentially from the pial migratory route use radial microvessels in an outside-in direction to populate superficial cortical layers (Léger et al., 2020a). At a mechanistic level, the endothelial NMDA receptor contributes to the control of this migration process by activating MMP9 activity (Léger et al., 2020a). Similarly, cortical oligodendrocytes are generated in ganglionic eminences (Kessaris et al., 2006). As demonstrated by Tsai and coworkers, these cells use periventricular microvessels to tangentially reach the corpus callosum and, subsequently, cortical layers (Tsai et al., 2016). At a mechanistic level, strong communication between endothelial cells and oligodendrocytes, including activation of the Wnt pathway, has been reported (Tsai et al., 2016; Yuen et al., 2014). For example, a reduction in Wnt activity induced an altered angiogenic response resulting in white matter defects (Chavali et al., 2020). In the present study, a 3D-modelization approach was performed on cortices from human fetuses and mouse neonates and showed that up to 15% and 40% of Olig2-positive cells were associated with radial microvessels, respectively. Although additional experiments, such as time-lapse studies, would be interesting, these data suggest that, as recently shown for GABAergic interneurons, radial cortical microvessels constitute a migration support for immature oligodendrocytes entering the neocortex.

4.2. Effects of prenatal alcohol exposure on cortical vasculature and vessel-associated oligodendrocytes

In humans, consumption of alcohol by pregnant women is frequently associated with a polyintoxication behavior associated with alcohol, tobacco, and cannabis (Forray, 2016). To clarify the effects of alcohol exposure on brain vasculature and Olig2-vessel association, we used a previously characterized TCAF-like mono-intoxication preclinical model (Jégou et al., 2012; Lecuyer et al., 2017; Léger et al., 2020b). In particular, alcohol exposure during the last days of mouse gestation (GD15 to birth) induces cortical vascular impairments without the characteristic facial dysmorphisms described in FAS models (Petrelli et al., 2018). Surprisingly, a time-course study of cortical vascular development at three developmental stages (E20, P2 and P15) revealed that PAE impaired the cortical vasculature at E20 and P2 but that this effect was no longer observed at P15. A possible interpretation of these data would be that the absence of alcohol exposure from P2 to P15, at a period where cortical angiogenesis is still occurring (Harb et al., 2013), attempted vascular impairments. To test this hypothesis, it would be interesting to investigate whether early postnatal alcohol exposure (from P3 to P15), corresponding to the third trimester of pregnancy in humans, could durably impair cortical microvasculature (Kelly et al., 1990; Xu et al., 2018).

Several studies from the literature established that *in utero* alcohol exposure impaired the survival and positioning of different cell types,

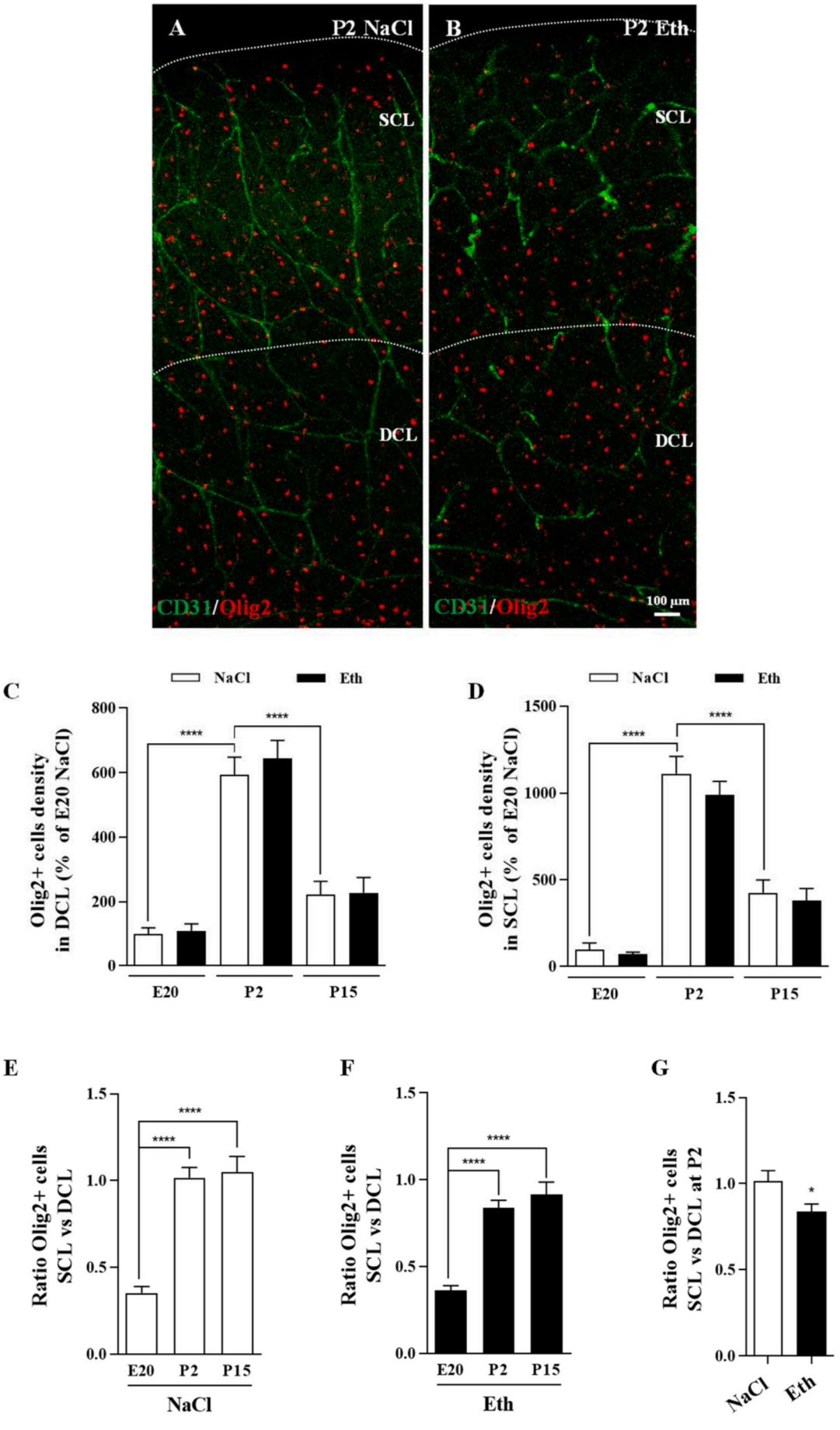

(caption on next page)

Fig. 4. Effects of PAE on the whole density of Olig2-positive cells in the developing cortex. A, B. Visualization of Olig2-positive cells in the developing cortex at P2 of control (A) and alcohol-exposed (B) fetuses. Olig2-positive cells were observed in both superficial (SCL) and deep (DCL) cortical layers. Microvessels were visualized using CD31 immunolabeling. C, D. Time course of the density of Olig2-positive cells in deep (C) and superficial (D) cortical layers of control (white bars) and *in utero* alcohol-exposed mice (black bars) at E20, P2 and P15. E, F. Ratio of Olig2-positive cell densities between superficial and deep cortical layers in control (E) and *in utero* alcohol-exposed mice (black bars) at E20, P2 and P15. G. Comparison of the SCL/DCL ratio between the control and alcohol groups at P2. ****$p < 0.0001$, two-way ANOVA followed by Tukey's post-test; *$p < 0.05$ *vs.* control using the unpaired t-test. DCL: deep cortical layers; SCL: superficial cortical layers; Eth: Ethanol.

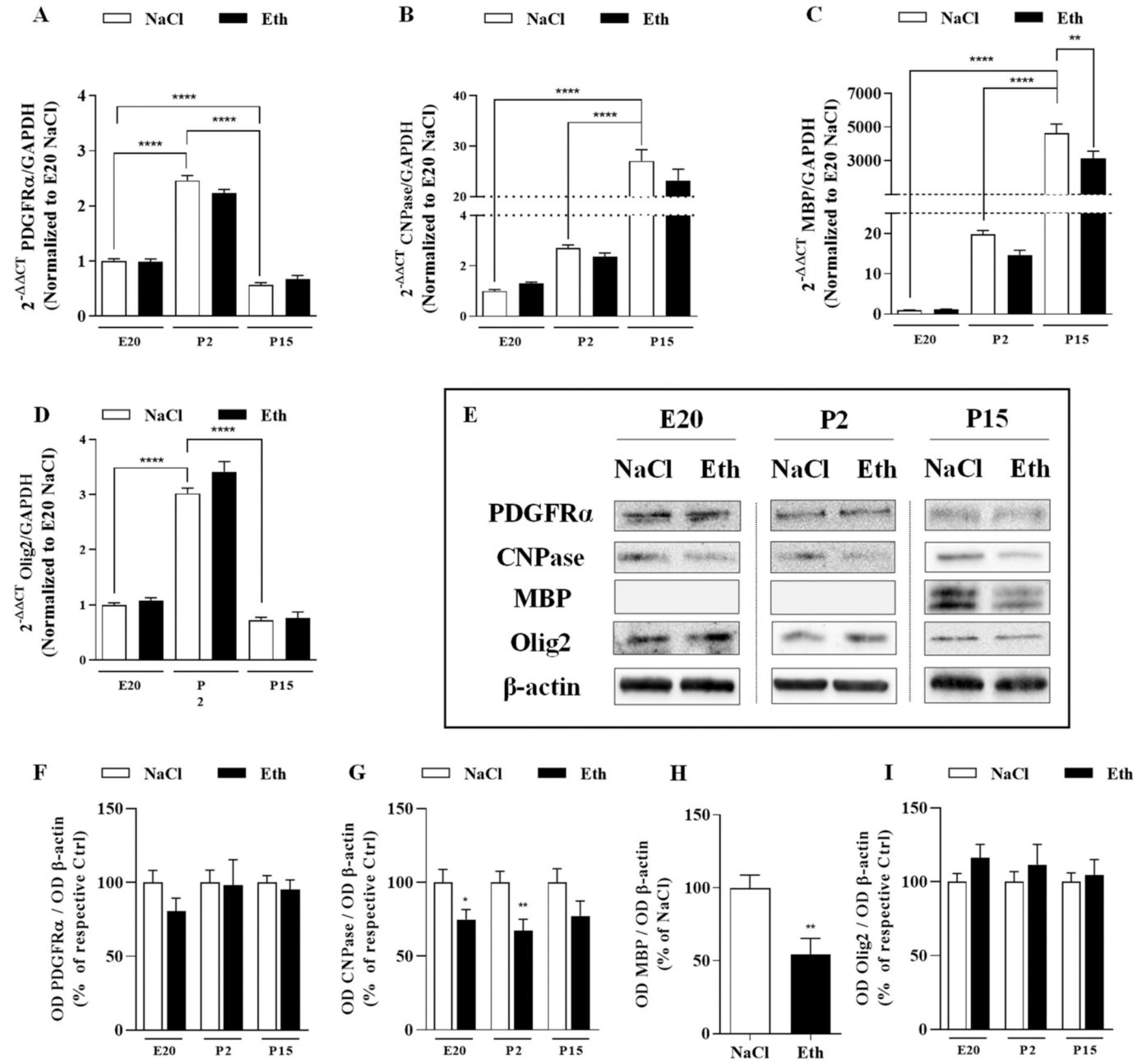

Fig. 5. Effects of PAE on the expression of differentiation markers of the oligodendrocyte lineage. A-D. Effect of PAE on PDGFRα (A), CNPase (B), MBP (C) and Olig2 (D) mRNA expression levels in cortical extracts from control (white bars) and *in utero* alcohol-exposed mice (black bars) at E20, P2 and P15. ****$p < 0.0001$, **$p < 0.01$ *vs.* control, two-way ANOVA followed by Tukey's post-test. *E*-I. Effect of PAE on PDGFRα (E, F), CNPase (E, G), MBP (E, H) and Olig2 (E, I) protein expression in cortical extracts from control (white bars) and *in utero* alcohol-exposed mice (black bars) at E20, P2 and P15. MBP was not detected by western blot at E20 and P2. *p < 0.05, **p < 0.01 *vs.* control using the unpaired t-test.

such as interneurons (Léger et al., 2020b) and oligodendrocytes (Creeley et al., 2013). However, considering that migration of these two cell types is vessel associated (Dejana and Betsholtz, 2016; Tsai et al., 2016), we explored whether PAE could impair the vessel association of oligodendrocytes. Data revealed that, regardless of the stage considered from E20 to P15 and despite vascular disorganization, *in utero* alcohol exposure did not modify the proportion of Olig2-positive cells associated with cortical microvessels. Altogether, these results suggest that *i)* the recruitment process of oligodendrocytes with microvessels is not affected by alcohol and *ii)* if oligodendrocytes remain vessel associated

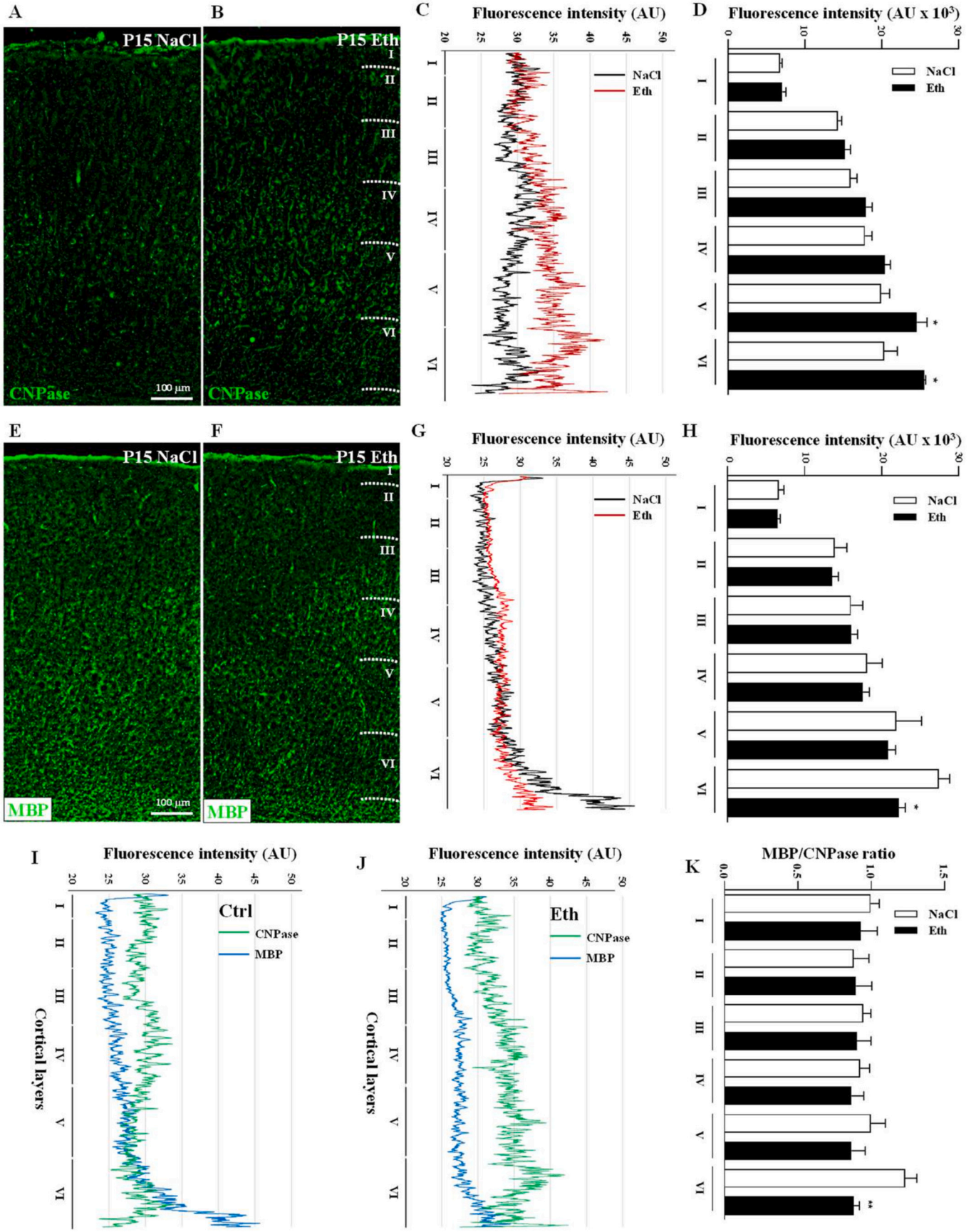

(caption on next page)

Fig. 6. Effects of PAE on the cortical distribution profile of CNPase and MBP immunoreactivities. A, B. Visualization of CNPase-positive cells in the developing cortex of control (A) and *in utero* alcohol-exposed (B) mice at P15. C. Distribution profiles by scanline analysis of CNPase immunoreactivity in cortical layers of control (black curve) and *in utero* alcohol-exposed (red curve) mice at P15. D. Quantification of the relative distribution of CNPase immunoreactivity between the cortical layers of control (white bars) and *in utero* alcohol-exposed (black bars) mice at P15. E, F. Visualization of MBP-positive cells in the developing cortex of control (E) and *in utero* alcohol-exposed (F) mice at P15. G. Distribution profiles by scanline analysis of MBP immunoreactivity in the cortical layers of control (black curve) and *in utero* alcohol-exposed (red curve) mice at P15. H. Quantification of the relative distribution of MBP immunoreactivity between cortical layers of control (white bars) and *in utero* alcohol-exposed (black bars) mice at P15. I, J. Comparison of the CNPase (green curves) and MBP (blue curves) distribution profiles in control (I) and *in utero* alcohol-exposed (J) mice at P15. K. Comparison of the MBP/CNPase ratio in the cortical layers from control (white bars) and *in utero* alcohol-exposed (black bars) mice at P15. *$p < 0.05$, **p < 0.01 *vs.* control using unpaired *t*-test. Crtl: Control; Eth: Ethanol. (For interpretation of the references to color in this figure legend, the reader is referred to the web version of this article.)

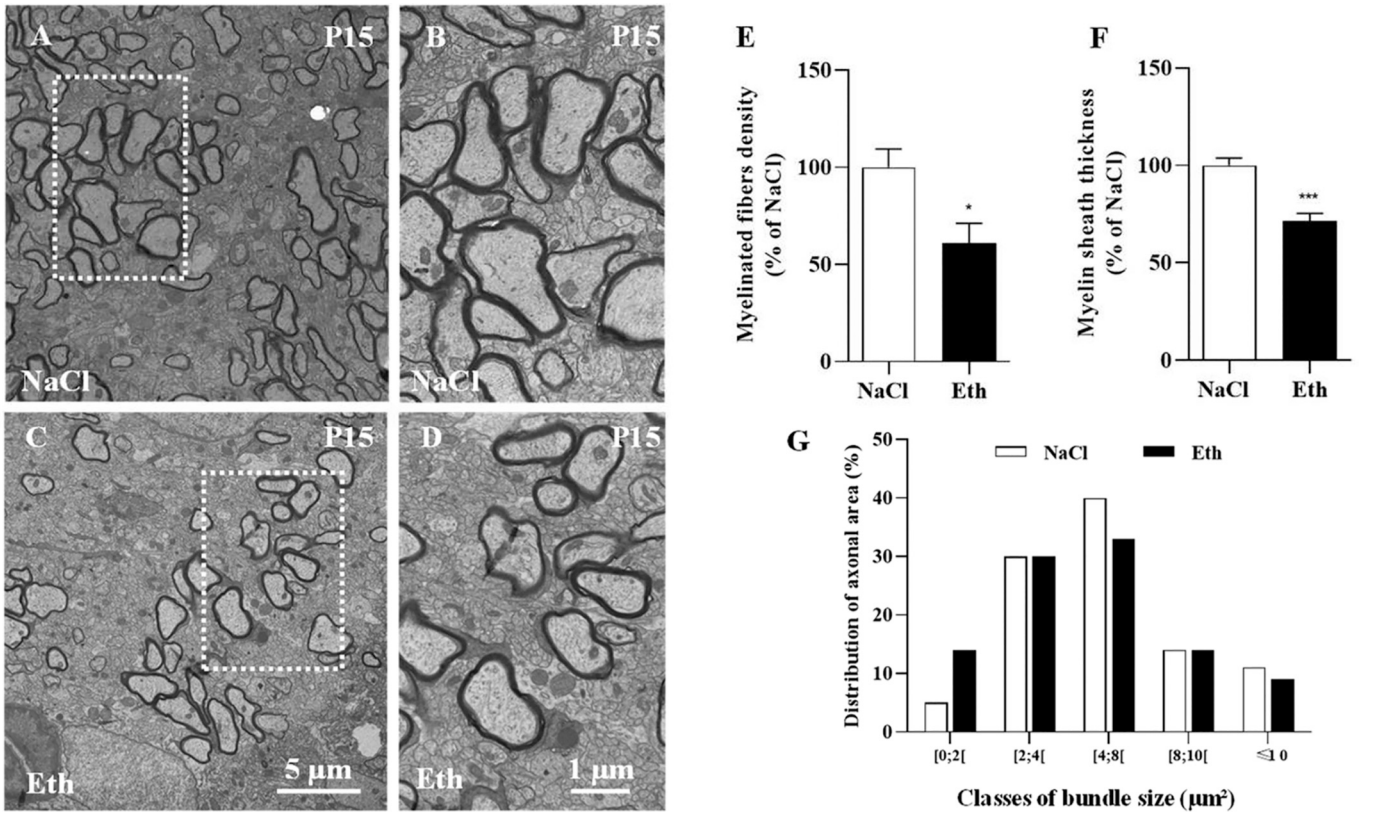

Fig. 7. Effects of PAE on axonal myelination in the corpus callosum. A-D. Visualization by electronic microscopy of myelinated axons at low (A, C) and high (B, D) magnification in transverse sections of corpus callosums from control (A, B) and *in utero* alcohol-exposed mice at P15. E. Quantifications of the density of myelinated fibers in the corpus callosum of control (white bar) and *in utero* alcohol-exposed (black bar) mice at P15. *$p < 0.05$ *vs.* control using unpaired t-test. F. Quantification of the myelin sheath of axons in the corpus callosum of control (white bar) and *in utero* alcohol-exposed (black bar) mice at P15. ***$p < 0.001$ *vs.* control using unpaired *t*-test. G. Distribution of myelinated axon areas in the corpus callosum of control (white bar) and *in utero* alcohol-exposed (black bar) mice at P15. Areas of axonal sections were distributed in 5 classes ranging from]0;2] to >10 µm^2. Statistical analysis was performed using the $\chi 2$ test. NaCl: Control; Eth: Ethanol.

and the microvascular network disorganized, then the positioning of Olig2-positive cells could be impaired.

4.3. PAE induced transient oligodendrocyte mispositioning in cortical layers

During brain development, the vascular network is established before OPC emergence (Daneman et al., 2009). Therefore, alcohol-induced vascular defects could lead to an incorrect migratory route for nervous cells. Consistent with this hypothesis, it has been recently shown that PAE induces a mispositioning of GABAergic interneurons in human and mouse models (Léger et al., 2020b; Marguet et al., 2020). Using preclinical models, it was shown that alcohol in addition to disorganizing microvessels impaired the activity of endothelial cells, such as glutamate-induced calcium mobilization and *in situ* activation of endothelial metalloproteinases (MMP9; Léger et al., 2020a). These effects were, at least in part, mimicked by invalidation of the endothelial NMDA receptor (Léger et al., 2020b). Consistent with these data, our experiments showed an imbalance of Olig2-positive cells in the developing cortex at birth (P2). After PAE, a greater proportion of oligodendrocytes was found in deep cortical layers compared with superficial cortical layers. Again, as noted for microvasculature, this effect was significant at P2 and attenuated at P15 if still observed. Altogether, these data suggest that ethanol delayed the positioning of oligodendrocytes entering cortical layers in our model of PAE.

4.4. PAE impaired the differentiation profile of cortical oligodendrocytes

To determine whether the effects of PAE on the cortical distribution of oligodendrocytes were associated with differentiation defects, we explored the expression and distribution of PDGFRα, CNPase and MBP, which are representative of different maturation stages of the lineage (Barateiro et al., 2016). Western blot analyses revealed that PAE markedly reduced the expression of CNPase, a myelin-associated enzyme, and MBP, a major constituent of the myelin sheath (Barateiro et al., 2016). Again, these effects were stage dependent. Specifically,

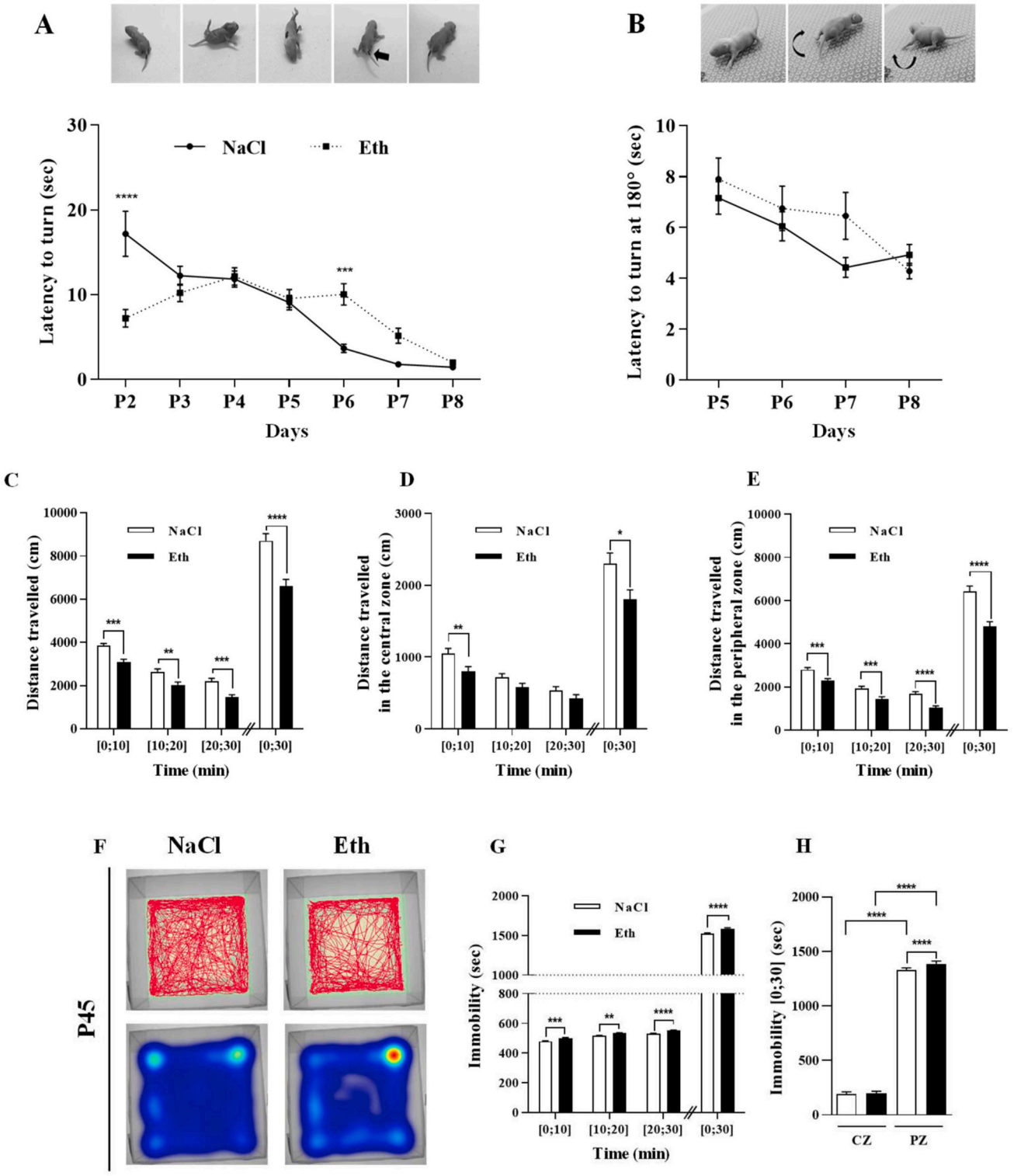

Fig. 8. Effects of PAE on sensorimotor disabilities. A. Time course quantification of the latency to turn from supine to prone position of control (black line) and alcohol-exposed (dotted line) neonates. The righting reflex test was performed from P2 to P8. ***p < 0.001, ****$p < 0.0001$ *vs.* control group using two-way ANOVA followed by Tukey's post-test. B. Time course quantification of the latency to turn from face-down to face-up position of control (black line) and alcohol-exposed (dotted line) neonates. The negative geotaxis tests were performed from P5 to P8. Statistical analysis was performed using two-way ANOVA followed by Tukey's post-test. C—F. Quantification of the distance travelled by control (white bars) and *in utero* alcohol-exposed (black bars) mice at P45. Distance covered was measured during the first 30 min of recording and analysed in the whole (C), central (D) and peripheral (E) zones of the open field. F. Visualization of the tracking and heatmaps used to quantify the distance travelled and immobility of control (NaCl) and *in utero* alcohol-exposed (Alcohol) mice at P45. The false color scale visualizes low (blue) and high (red) durations of immobility. G, H. Quantification of immobility of control (white bars) and *in utero* alcohol-exposed (black bars) mice at P45. Immobility was measured during the first 30 min of recording and analysed in the whole (G), central (H) and peripheral (H) zones of the open field. *$p < 0.05$, **$p < 0.01$, ***$p < 0.001$, ****p < 0.0001 *vs.* control using two-way ANOVA followed by Tukey's post-test and unpaired t-test. (For interpretation of the references to color in this figure legend, the reader is referred to the web version of this article.)

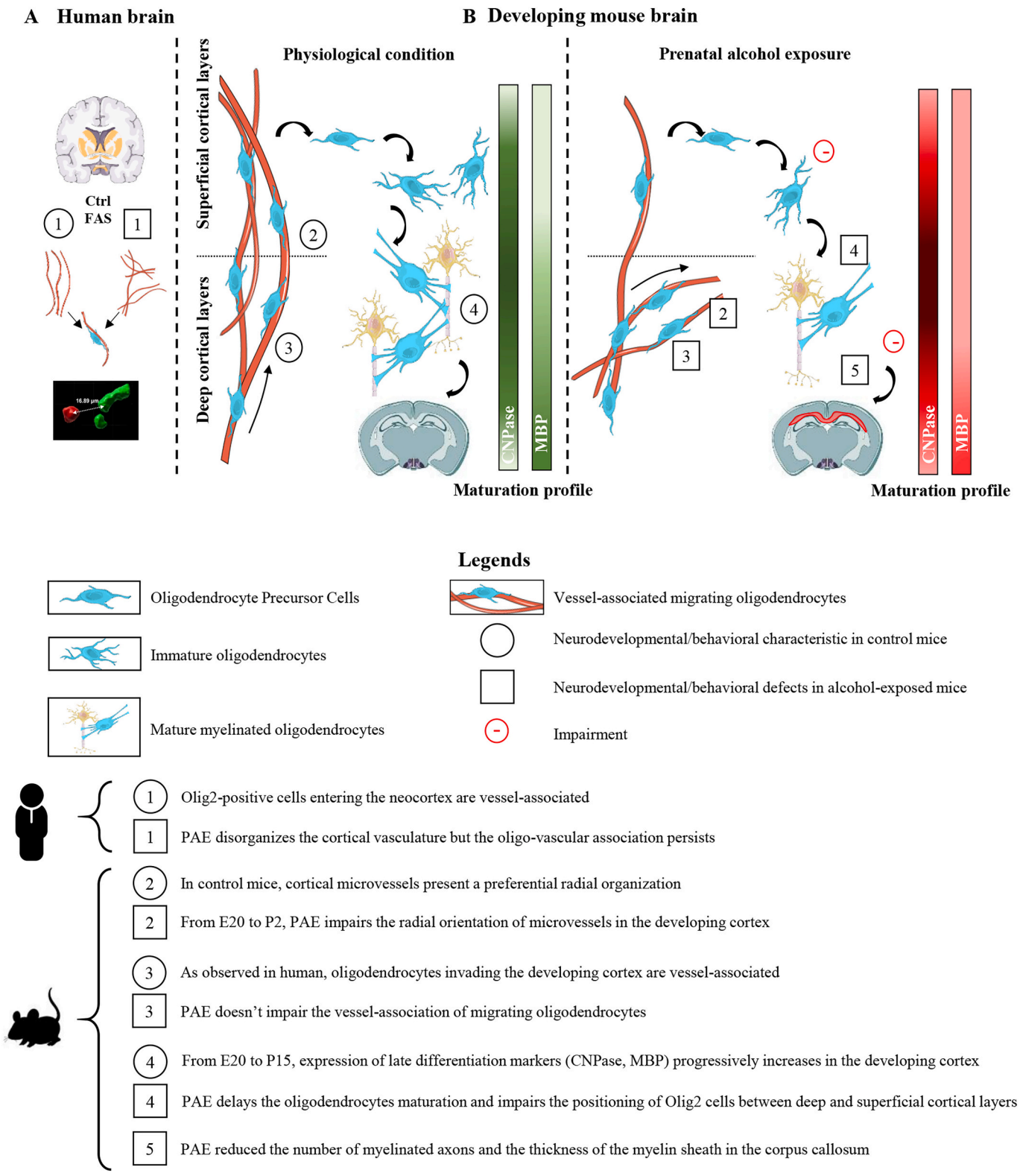

Fig. 9. Graphical abstract integrating neurodevelopmental highlights in humans (A) and mice (B). Data from non-exposed and *in utero*-exposed to alcohol are represented by circled and squared numbers, respectively. Each symbol is described in the graph legend.

CNPase reduction was maximum at P2, whereas the effect of PAE on MBP was first found at P15 and vanished in adulthood. As suggested by transient vascular impairments and transient Olig2 positioning, these data support a delay in the late differentiation of oligodendrocytes. Consistent with these results, Cantacorps et al. (2017) also found a reduction in several myelin markers after prenatal and early neonatal alcohol exposure in mice. Similarly, late exposure to alcohol in a binge drinking model also reduced myelin marker expression (Rice and Gu, 2019), indicating a high sensitivity of oligodendrocytes to ethanol regardless of the alcohol exposure protocol. Even if performed from

microdissected extracts, RT–PCR and western blot experiments do not inform on the cortical maturation profile of oligodendrocytes. Focusing on immature (CNPase positive) and mature (MBP positive) oligodendrocytes, scanline analysis was performed in the developing cortex at P15 and showed that the highest level of intensity profiles corresponding to mature oligodendrocytes was found in cortical layers V and VI (Tan et al., 2009). PAE reversed the CNPase and MBP intensity profiles, especially in layer VI, suggesting that the effects of alcohol on CNPase and MBP expression affected cell populations present in layer VI. Data from Southwell and co-workers revealed that, during cortical development, cell fate of GABAergic interneurons entering the developing cortex is under control of trophic factors (Southwell et al., 2012). The present study provides first evidence that, as recently discovered for GABAergic interneurons (Léger et al., 2020a), there is a vascular association of oligodendrocytes entering the neocortex. Consequently, the present study raises the hypothesis of a functional link between impaired vessel-associated migration and impaired differentiation of oligodendrocytes after PAE. Supporting this hypothesis, it has been recently shown using $Grin1^{lox/lox}$-$VeCad^{Cre}$ mice that the endothelial NMDA receptor is involved in cell fate of GABAergic interneurons (Léger et al., 2020a). Among new research avenues it would be tempting to investigate if in $Grin1^{lox/lox}$-$VeCad^{Cre}$ transgenic mice the differentiation of oligodendrocytes is impaired. Interestingly, two recent clinical studies including one of our research group revealed an increase in progenitor markers and a decrease in mature oligodendrocyte markers in the brains of human fetuses prenatally exposed to alcohol (Darbinian et al., 2021; Marguet et al., 2022). Altogether, these data indicate that the mispositioning of Olig2-positive cells observed in deep cortical layers after PAE is associated with an immature-like oligodendrocyte profile.

4.5. *PAE induced transient white matter damage but long-term locomotor impairments*

Axon myelination is required for correct nerve impulse conduction, neuronal integrity and metabolic support (Fields and Dutta, 2019; Philips and Rothstein, 2017). In humans, it has long been established that *in utero* alcohol exposure alters corpus callosum formation, leading to global white matter reduction (Sowell et al., 2002) as well as callosal agenesis in the more severe cases (Lebel et al., 2011; Riley et al., 1995). The present data revealed that at P15, PAE induced a significant reduction in *i)* MBP expression in cortical layers, *ii)* a reduction in myelin sheath and axonal sections in the corpus callosum and *iii)* a disorganization of myelinated bundles in the striatum, a corticofugal target. Again, as found for microvasculature disorganization, the effects of PAE on MBP expression and myelinated bundles were not retrieved in adult mice, supporting a recovery process. Interestingly, a recent study showed a very similar disorganization of axonal fibers in the rat corpus callosum after alcohol exposure (Newville et al., 2022). However, two main differences emerged between the two studies. First, contrasting with our data, the myelination impairments persisted in adult rats in the study from Newville and coworkers. Second, the authors used a postnatal (P3-P15) window of exposure rather than a prenatal (E15-Birth) window, as we did. Altogether, these data suggest that the later the exposure occurred, the lower the recovery.

In humans, FAS corresponds to the more severe expression of FASD and is characterized by morphological abnormalities, such as facial dimorphism (Riley et al., 2011); neurodevelopmental impairments, such as reduction of the corpus callosum volume (Darbinian and Selzer, 2022), and behavioral troubles (De Ávila et al., 2020; Kleiber et al., 2011). Using fine morphometric and imagery tools, several research groups have tried to correlate dysmorphism and/or neurodevelopmental defects with behavioral disorders to improve diagnosis (Biffen et al., 2018; Fan et al., 2016). However, the early diagnosis of FASD remains challenging, and numerous infants are still undiagnosed until school age (Chasnoff et al., 2015). Interestingly, the present data showed, using a FASD model of prenatal alcohol exposure, that neonates who presented marked perinatal oligovascular impairments subsequently developed long-term behavioral deficits (reduced locomotor activity; Cantacorps et al., 2017).

Although they are few, some clinical studies compared the effects of PAE between girls and boys (Uban et al., 2017; May et al., 2017). Even if both genders had mostly similar outcomes (May et al., 2017), considering white matter microstructures, data from Uban and co-workers revealed that girls with PAE exhibited lower fractional anisotropy, an indicator of impaired myelination (Uban et al., 2017). In the present study, qRT-PCR, western blot, and behavioral experiments were performed considering females and males. Consistent with clinic, results showed similar trajectories between females and males. However, fine sex differences were observed. In particular, qRT-PCR and western blot experiments showed that, during the first two postnatal weeks, the inhibitory effect of PAE on MBP expression was more pronounced in female mice. Because perinatal life is a critical period for sexual differentiation of the brain (Lenz et al., 2012). These data suggest that environmental-induced defects occurring during perinatal life may result in gender-specific disabilities (VanRyzin et al., 2020).

In conclusion, it is now well established that prenatal alcohol exposure represents a main cause of neurobehavioral troubles. Numerous studies have focused on nerve cells, ignoring the recently evidenced neurovascular dysfunction. On the one hand, cortical microvessels are altered by PAE both in humans and mice. On the other hand, oligodendrocytes require microvessels to reach the neocortex from ganglionic eminences. Using an *in utero* exposure model of FASD, the present study provides the first evidence that PAE induced a transient disorganization of the cortical microvasculature, whereas the vessel association of immature oligodendrocytes was preserved. Concomitantly, a mispositioning and a delayed differentiation profile of oligodendrocytes were observed in cortical layers. Whereas most of these morphometric and developmental parameters were transient and observed in the first two postnatal weeks, offspring will develop long-term motor behavioral deficits. Altogether, these data support that alcohol-induced vascular defects recently described in human neonates may provide new research avenues for the early diagnosis of FASD in infants. Supplementary figures for this article can be found online.

Supplementary data to this article can be found online at https://doi.org/10.1016/j.nbd.2022.105791.

Support

This work was supported by Normandy University, Rouen University, Institut National de la Santé et de la Recherche Médicale (INSERM, UMR1245; UMR-S U1237), Rouen University Hospital, Fondation de France, Blood & Brain Institute, ANR AlcoBrain, and the Normandy Region. MB was a recipient of a fellowship from the French Research Ministry of Research and Higher Education.

CRediT authorship contribution statement

M. Brosolo: Conceptualization, Investigation. **M. Lecointre:** Conceptualization, Investigation. **A. Laquerrière:** Conceptualization. **F. Janin**: Investigation, Methodology. **D. Genty**: Investigation, Methodology. **A. Lebon**: Investigation, Methodology. **C. Lesueur**: Methodology. **D. Vivien:** Funding acquisition. **S. Marret:** Conceptualization. **F. Marguet:** Conceptualization. **B.J. Gonzalez:** Conceptualization, Supervision, Funding acquisition.

Declaration of Competing Interest

None.

References

Barateiro, A., Brites, D., Fernandes, A., 2016. Oligodendrocyte development and myelination in neurodevelopment: molecular mechanisms in health and disease. Curr. Pharm. Des. 22, 656–679.

Biffen, S.C., Warton, C.M.R., Lindinger, N.M., Randall, S.R., Lewis, C.E., Molteno, C.D., Jacobson, J.L., Jacobson, S.W., Meintjes, E.M., 2018. Reductions in Corpus callosum volume partially mediate effects of prenatal alcohol exposure on IQ. Front. Neuroanat. 11, 132.

Byers, S.L., Wiles, M.V., Dunn, S.L., Taft, R.A., 2012. Mouse estrous cycle identification tool and images. PLoS One 7, e35538.

Cantacorps, L., Alfonso-Loeches, S., Moscoso-Castro, M., Cuitavi, J., Gracia-Rubio, I., López-Arnau, R., Escubedo, E., Guerri, C., Valverde, O., 2017. Maternal alcohol binge drinking induces persistent neuroinflammation associated with myelin damage and behavioural dysfunctions in offspring mice. Neuropharmacology. 123, 368–384.

Chasnoff, I.J., Wells, A.M., King, L., 2015. Misdiagnosis and missed diagnoses in foster and adopted children with prenatal alcohol exposure. Pediatrics. 135, 264–270.

Chavali, M., Ulloa-Navas, M.J., Pérez-Borredá, P., Garcia-Verdugo, J.M., McQuillen, P.S., Huang, E.J., Rowitch, D.H., 2020. Wnt-dependent oligodendroglial-endothelial interactions regulate white matter vascularization and attenuate injury. Neuron 108, 1130–1145.e5.

Choe, Y., Huynh, T., Pleasure, S.J., 2014. Migration of oligodendrocyte progenitor cells is controlled by transforming growth factor β family proteins during corticogenesis. J. Neurosci. 34, 14973–14983.

Creeley, C.E., Dikranian, K.T., Johnson, S.A., Farber, N.B., Olney, J.W., 2013. Alcohol-induced apoptosis of oligodendrocytes in the fetal macaque brain. Acta Neuropathol Commun. 1, 23.

Daher, I., Le Dieu-Lugon, B., Dourmap, N., Lecuyer, M., Ramet, L., Gomila, C., Ausseil, J., Marret, S., Leroux, P., Roy, V., El Mestikawy, S., Daumas, S., Gonzalez, B., Leroux-Nicollet, I., Cleren, C., 2017. Magnesium sulfate prevents neurochemical and long-term behavioral consequences of neonatal Excitotoxic lesions: comparison between male and female mice. J. Neuropathol. Exp. Neurol. 76, 883–897.

Dalitz, P., Cock, M., Harding, R., Rees, S., 2008. Injurious effects of acute ethanol exposure during late gestation on developing white matter in fetal sheep. Int. J. Dev. Neurosci. 26, 391–399.

Daneman, R., Agalliu, D., Zhou, L., Kuhnert, F., Kuo, C.J., Barres, B.A., 2009. Wnt/beta-catenin signaling is required for CNS, but not non-CNS, angiogenesis. Proc Natl Acad Sci USA. 106:641-6. In: Erratum in: Proc Natl Acad Sci USA. 2009, 106, p. 6422.

Darbinian, N., Selzer, M.E., 2022. Oligodendrocyte pathology in fetal alcohol spectrum disorders. Neural Regen. Res. 17, 497–502.

Darbinian, N., Darbinyan, A., Merabova, N., Bajwa, A., Tatevosian, G., Martirosyan, D., Zhao, H., Selzer, M.E., Goetzl, L., 2021. Ethanol-mediated alterations in oligodendrocyte differentiation in the developing brain. Neurobiol. Dis. 148, 105181.

De Ávila, M.A.P., Gonçalves, R.M., Nascimento, E.C.C., Cabral, L.D.M., Vilela, F.C., Giusti-Paiva, A., 2020. Prenatal exposure to alcohol impairs social play behavior in adolescent male mice. Neurotoxicology. 79, 142–149.

Dejana, E., Betsholtz, C., 2016. NEURODEVELOPMENT. Oligodendrocytes follow blood vessel trails in the brain. Science. 351, 341–342.

Donald, K.A., Eastman, E., Howells, F.M., Adnams, C., Riley, E.P., Woods, R.P., Narr, K. L., Stein, D.J., 2015. Neuroimaging effects of prenatal alcohol exposure on the developing human brain: a magnetic resonance imaging review. Acta Neuropsychiatr. 27, 251–269.

Fan, J., Jacobson, S.W., Taylor, P.A., Molteno, C.D., Dodge, N.C., Stanton, M.E., Jacobson, J.L., Meintjes, E.M., 2016. White matter deficits mediate effects of prenatal alcohol exposure on cognitive development in childhood. Hum. Brain Mapp. 37, 2943–2958.

Fields, R.D., Dutta, D.J., 2019. Treadmilling model for plasticity of the myelin sheath. Trends Neurosci. 42, 443–447.

Forray, A., 2016. Substance use during pregnancy. F1000Res. 5:F1000 Faculty Rev-887.

Harb, R., Whiteus, C., Freitas, C., Grutzendler, J., 2013. In vivo imaging of cerebral microvascular plasticity from birth to death. J. Cereb. Blood Flow Metab. 33, 146–156.

Jäkel, S., Dimou, L., 2017. Glial cells and their function in the adult brain: a journey through the history of their ablation. Front. Cell. Neurosci. 11, 24.

Jégou, S., El Ghazi, F., de Lendeu, P.K., Marret, S., Laudenbach, V., Uguen, A., Marcorelles, P., Roy, V., Laquerrière, A., Gonzalez, B.J., 2012. Prenatal alcohol exposure affects vasculature development in the neonatal brain. Ann. Neurol. 72, 952–960.

Kelly, S.J., Mahoney, J.C., West, J.R., 1990. Changes in brain microvasculature resulting from early postnatal alcohol exposure. Alcohol. 7, 43–47.

Kessaris, N., Fogarty, M., Iannarelli, P., Grist, M., Wegner, M., Richardson, W.D., 2006. Competing waves of oligodendrocytes in the forebrain and postnatal elimination of an embryonic lineage. Nat. Neurosci. 9, 173–179.

Kleiber, M.L., Wright, E., Singh, S.M., 2011. Maternal voluntary drinking in C57BL/6J mice: advancing a model for fetal alcohol spectrum disorders. Behav. Brain Res. 223, 376–387.

Lange, S., Probst, C., Gmel, G., Rehm, J., Burd, L., Popova, S., 2017. Global prevalence of fetal alcohol Spectrum disorder among children and youth: a systematic review and Meta-analysis. JAMA Pediatr. 171, 948–956.

Lebel, C., Roussotte, F., Sowell, E.R., 2011. Imaging the impact of prenatal alcohol exposure on the structure of the developing human brain. Neuropsychol. Rev. 21, 102–118.

Lecuyer, M., Laquerrière, A., Bekri, S., Lesueur, C., Ramdani, Y., Jégou, S., Uguen, A., Marcorelles, P., Marret, S., Gonzalez, B.J., 2017. PLGF, a placental marker of fetal brain defects after in utero alcohol exposure. Acta Neuropathol Commun. 5, 44.

Léger, C., Dupré, N., Aligny, C., Bénard, M., Lebon, A., Henry, V., Hauchecorne, M., Galas, L., Frebourg, T., Leroux, P., Vivien, D., Lecointre, M., Marret, S., Gonzalez, B. J., 2020a. Glutamate controls vessel-associated migration of GABA interneurons from the pial migratory route via NMDA receptors and endothelial protease activation. Cell. Mol. Life Sci. 77, 1959–1986.

Léger, C., Dupré, N., Laquerrière, A., Lecointre, M., Dumanoir, M., Janin, F., Hauchecorne, M., Fabre, M., Jégou, S., Frébourg, T., Cleren, C., Leroux, P., Marcorelles, P., Brasse-Lagnel, C., Marret, S., Marguet, F., Gonzalez, B.J., 2020b. In utero alcohol exposure exacerbates endothelial protease activity from pial microvessels and impairs GABA interneuron positioning. Neurobiol. Dis. 145, 105074.

Lenz, K.M., Nugent, B.M., McCarthy, M.M., 2012. Sexual differentiation of the rodent brain: dogma and beyond. Front. Neurosci. 6, 26.

Li, J., Li, C., Loreno, E.G., Miriyala, S., Panchatcharam, M., Lu, X., Sun, H., 2021. Chronic low-dose alcohol consumption promotes cerebral angiogenesis in mice. Front Cardiovasc Med. 8, 681627.

Luhmann, H.J., Fukuda, A., Kilb, W., 2015. Control of cortical neuronal migration by glutamate and GABA. Front. Cell. Neurosci. 9, 4.

Marguet, F., Friocourt, G., Brosolo, M., Sauvestre, F., Marcorelles, P., Lesueur, C., Marret, S., Gonzalez, B.J., Laquerrière, A., 2020. Prenatal alcohol exposure is a leading cause of interneuronopathy in humans. Acta Neuropathol Commun. 8, 208.

Marguet, F., Brosolo, M., Friocourt, G., Sauvestre, F., Marcorelles, P., Lesueur, C., Marret, S., Gonzalez, B.J., Laquerrière, A., 2022. Oligodendrocyte lineage is severely affected in human alcohol-exposed foetuses. Acta Neuropathol Commun. 10, 74.

Marinelli, C., Bertalot, T., Zusso, M., Skaper, S.D., Giusti, P., 2016. Systematic review of pharmacological properties of the oligodendrocyte lineage. Front. Cell. Neurosci. 10, 27.

Mattson, S.N., Crocker, N., Nguyen, T.T., 2011. Fetal alcohol spectrum disorders: neuropsychological and behavioral features. Neuropsychol. Rev. 21, 81–101.

May, P.A., Tabachnick, B., Hasken, J.M., Marais, A.S., de Vries, M.M., Barnard, R., Joubert, B., Cloete, M., Botha, I., Kalberg, W.O., Buckley, D., Burroughs, Z.R., Bezuidenhout, H., Robinson, L.K., Manning, M.A., Adnams, C.M., Seedat, S., Parry, C.D.H., Hoyme, H.E., 2017. Who is most affected by prenatal alcohol exposure: boys or girls? Drug Alcohol Depend. 177, 258–267.

Newville, J., Valenzuela, C.F., Li, L., Jantzie, L.L., Cunningham, L.A., 2017. Acute oligodendrocyte loss with persistent white matter injury in a third trimester equivalent mouse model of fetal alcohol spectrum disorder. Glia. 65, 1317–1332.

Newville, J., Howard, T.A., Chavez, G.J., Valenzuela, C.F., Cunningham, L.A., 2022. Persistent myelin abnormalities in a third trimester-equivalent mouse model of fetal alcohol spectrum disorder. Alcohol. Clin. Exp. Res. 46, 77–86.

Nishiyama, A., Shimizu, T., Sherafat, A., Richardson, W.D., 2021. Life-long oligodendrocyte development and plasticity. Semin. Cell Dev. Biol. 116, 25–37.

Niu, J., Yu, G., Wang, X., Xia, W., Wang, Y., Hoi, K.K., Mei, F., Xiao, L., Chan, J.R., Fancy, S.P.J., 2021. Oligodendroglial ring finger protein Rnf43 is an essential injury-specific regulator of oligodendrocyte maturation. Neuron. 109, 3104–3118.e6.

Paredes, I., Himmels, P., Ruiz de Almodóvar, C., 2018. Neurovascular communication during CNS development. Dev. Cell 45, 10–32.

Petrelli, B., Weinberg, J., Hicks, G.G., 2018. Effects of prenatal alcohol exposure (PAE): insights into FASD using mouse models of PAE. Biochem. Cell Biol. 96, 131–147.

Philips, T., Rothstein, J.D., 2017. Oligodendroglia: metabolic supporters of neurons. J. Clin. Invest. 127, 3271–3280.

Popova, S., Lange, S., Shield, K., Burd, L., Rehm, J., 2019. Prevalence of fetal alcohol spectrum disorder among special subpopulations: a systematic review and meta-analysis. Addiction. 114, 1150–1172.

Radek, K.A., Matthies, A.M., Burns, A.L., Heinrich, S.A., Kovacs, E.J., Dipietro, L.A., 2005. Acute ethanol exposure impairs angiogenesis and the proliferative phase of wound healing. Am. J. Physiol. Heart Circ. Physiol. 289, H1084–H1090.

Radek, K.A., Kovacs, E.J., Gallo, R.L., DiPietro, L.A., 2008. Acute ethanol exposure disrupts VEGF receptor cell signaling in endothelial cells. Am. J. Physiol. Heart Circ. Physiol. 295, H174–H184.

Rice, J., Gu, C., 2019. Function and mechanism of myelin regulation in alcohol abuse and alcoholism. Bioessays. 41, e1800255.

Riley, E.P., Mattson, S.N., Sowell, E.R., Jernigan, T.L., Sobel, D.F., Jones, K.L., 1995. Abnormalities of the corpus callosum in children prenatally exposed to alcohol. Alcohol. Clin. Exp. Res. 19, 1198–1202.

Riley, E.P., Infante, M.A., Warren, K.R., 2011. Fetal alcohol spectrum disorders: an overview. Neuropsychol. Rev. 21, 73–80.

Roux, C., Lesueur, C., Aligny, C., Brasse-Lagnel, C., Genty, D., Marret, S., Laquerrière, A., Bekri, S., Gonzalez, B.J., 2014. 3-MA inhibits autophagy and favors long-term integration of grafted Gad67-GFP GABAergic precursors in the developing neocortex by preventing apoptosis. Cell Transplant. 23, 1425–1450.

Southwell, D.G., Paredes, M.F., Galvao, R.P., Jones, D.L., Froemke, R.C., Sebe, J.Y., Alfaro-Cervello, C., Tang, Y., Garcia-Verdugo, J.M., Rubenstein, J.L., Baraban, S.C., Alvarez-Buylla, A., 2012. Intrinsically determined cell death of developing cortical interneurons. Nature. 491, 109–113.

Sowell, E.R., Thompson, P.M., Mattson, S.N., Tessner, K.D., Jernigan, T.L., Riley, E.P., Toga, A.W., 2002. Regional brain shape abnormalities persist into adolescence after heavy prenatal alcohol exposure. Cereb. Cortex 12, 856–865.

Sulik, K.K., 2014. Fetal alcohol spectrum disorder: pathogenesis and mechanisms. Handb. Clin. Neurol. 125, 463–475.

Syed, F., John, P.J., Soni, I., 2016. Neurodevelopmental consequences of gestational and lactational exposure to pyrethroids in rats. Environ. Toxicol. 31, 1761–1770.

Tan, S.S., Kalloniatis, M., Truong, H.T., Binder, M.D., Cate, H.S., Kilpatrick, T.J., Hammond, V.E., 2009. Oligodendrocyte positioning in cerebral cortex is independent of projection neuron layering. Glia. 57, 1024–1030.
Tsai, H.H., Niu, J., Munji, R., Davalos, D., Chang, J., Zhang, H., Tien, A.C., Kuo, C.J., Chan, J.R., Daneman, R., Fancy, S.P., 2016. Oligodendrocyte precursors migrate along vasculature in the developing nervous system. Science. 351, 379–384.
Uban, K.A., Herting, M.M., Wozniak, J.R., Sowell, E.R., CIFASD, 2017. Sex differences in associations between white matter microstructure and gonadal hormones in children and adolescents with prenatal alcohol exposure. Psychoneuroendocrinology. 83, 111–121.
Ueda, Y., Misumi, S., Suzuki, M., Ogawa, S., Nishigaki, R., Ishida, A., Jung, C.G., Hida, H., 2018. Disorganization of oligodendrocyte development in the layer II/III of the sensorimotor cortex causes motor coordination dysfunction in a model of white matter injury in neonatal rats. Neurochem. Res. 43, 136–146.
Usrey, W.M., Sherman, S.M., 2019. Corticofugal circuits: communication lines from the cortex to the rest of the brain. J. Comp. Neurol. 527, 640–650.
Van Tilborg, E., de Theije, C.G.M., van Hal, M., Wagenaar, N., de Vries, L.S., Benders, M. J., Rowitch, D.H., Nijboer, C.H., 2018. Origin and dynamics of oligodendrocytes in the developing brain: implications for perinatal white matter injury. Glia. 66, 221–238.
VanRyzin, J.W., Marquardt, A.E., Pickett, L.A., McCarthy, M.M., 2020. Microglia and sexual differentiation of the developing brain: a focus on extrinsic factors. Glia. 68, 1100–1113.
Volpe, J.J., 2009. Brain injury in premature infants: a complex amalgam of destructive and developmental disturbances. Lancet Neurol. 8, 110–124.
Williams, J.K., Baptista, P.M., Daunais, J.B., Szeliga, K.T., Friedman, D.P., Soker, S., 2008. The effects of ethanol consumption on vasculogenesis potential in nonhuman primates. Alcohol. Clin. Exp. Res. 32, 155–161.
Won, C., Lin, Z., Kumar, T.P., Li, S., Ding, L., Elkhal, A., Szabó, G., Vasudevan, A., 2013. Autonomous vascular networks synchronize GABA neuron migration in the embryonic forebrain. Nat. Commun. 4, 2149.
Wozniak, J.R., Muetzel, R.L., Mueller, B.A., McGee, C.L., Freerks, M.A., Ward, E.E., Nelson, M.L., Chang, P.N., Lim, K.O., 2009. Microstructural corpus callosum anomalies in children with prenatal alcohol exposure: an extension of previous diffusion tensor imaging findings. Alcohol. Clin. Exp. Res. 33, 1825–1835.
Xu, W., Hawkey, A.B., Li, H., Dai, L., Brim, H.H., Frank, J.A., Luo, J., Barron, S., Chen, G., 2018. Neonatal ethanol exposure causes behavioral deficits in young mice. Alcohol. Clin. Exp. Res. 42, 743–750.
Yuen, T.J., Silbereis, J.C., Griveau, A., Chang, S.M., Daneman, R., Fancy, S.P.J., Zahed, H., Maltepe, E., Rowitch, D.H., 2014. Oligodendrocyte-encoded HIF function couples postnatal myelination and white matter angiogenesis. Cell. 158, 383–396.